AGU100 ADVANCING EARTH AND SPACE SCIENCE

Geochemistry, Geophysics, Geosystems

RESEARCH ARTICLE
10.1029/2017GC007399

Key Points:
- The lithosphere thickens from ~200 km beneath central and southwestern Kaapvaal to ~300 km beneath the Limpopo Belt
- Surface elevation and lithospheric thickness anticorrelate; the relationship implies weakly depleted deep (200–300 km) Limpopo lithosphere
- Shear velocity increases from the Moho to 100–150 km depths; this can be explained by the gradual emergence of garnet below 80 km

Supporting Information:
- Supporting Information S1

Correspondence to:
M. Ravenna,
mravenna@cp.dias.ie

Citation:
Ravenna, M., Lebedev, S., Fullea, J., & Adam, J. M.-C. (2018). Shear-wave velocity structure of Southern Africa's lithosphere: Variations in the thickness and composition of cratons and their effect on topography. *Geochemistry, Geophysics, Geosystems*, *19*, 1499–1518. https://doi.org/10.1029/2017GC007399

Received 12 DEC 2017
Accepted 29 MAR 2018
Accepted article online 16 APR 2018
Published online 13 MAY 2018

Shear-Wave Velocity Structure of Southern Africa's Lithosphere: Variations in the Thickness and Composition of Cratons and Their Effect on Topography

Matteo Ravenna[1,2], Sergei Lebedev[1], Javier Fullea[1], and Joanne M.-C. Adam[3]

[1]School of Cosmic Physics, Geophysics Section, Dublin Institute for Advanced Studies, Dublin, Ireland, [2]School of Earth Sciences, University College Dublin, Belfield, Dublin, Ireland, [3]Institut de Physique du Globe, Paris, France

Abstract Seismic-wave velocities offer essential constraints on the temperature, thickness, and composition of the lithosphere of cratons. We invert broadband, Rayleigh-wave phase and Love-wave phase velocities measured across the Kaapvaal Craton and Limpopo Belt for depth distributions of shear-wave velocity and radial anisotropy, from the upper-crust down to deep upper mantle. Our probabilistic, Bayesian inversion addresses model nonuniqueness by means of direct parameter-space sampling. An increase in V_s between the Moho and 100–150 km depths occurs across the region and can be explained by the gradual emergence of garnet below 80 km, due to the spinel peridotite-garnet peridotite transformation and due to the exsolution of garnet from mantle orthopyroxene. Lateral variations in this V_s gradient can provide new information on lateral compositional variations. Cold cratonic lithosphere is manifest in very high shear velocities, up to 4.8 km/s. The depth extent of the shear-velocity anomaly and the inferred lithospheric thickness increase from ~200 km beneath the central and southwestern Kaapvaal to ~300 km beneath the Limpopo Belt. Curiously, surface elevation decreases monotonically with the increasing lithospheric thickness. The relationship between the lithospheric thickness and topography depends on the lithospheric composition and, with the crustal structure taken into account, our results imply that the bottom part of the Limpopo lithosphere (200–300 km) is weakly-to-moderately depleted (Mg# 89.7–90.8). Our results also show that the central-southwestern Kaapvaal lithosphere is thinner than it was (according to kimberlites) 100–200 m.y. ago. It may have been thinned by the same mantle plume that, initially, triggered the kimberlite eruptions.

Plain Language Summary Cratons, the ancient cores of continents, have an unusually thick lithosphere (the tectonic plate beneath them). At least ~200 km thick, it has a highly anomalous composition, making it less dense than the surrounding mantle. Cratonic lithosphere can thus be cooled to much lower temperatures than elsewhere. Variations in this delicate buoyancy balance probably give rise to variations in the surface elevation across the Earth's stable continents. Lithospheric thickness and composition are key parameters, but both are notoriously difficult to determine. Here we use very accurate measurements of seismic surface-wave velocities and determine deep structure beneath cratons in southern Africa. We discover an unexpectedly strong, gradual thickening of the lithosphere from the central Kaapvaal Craton to the neighboring Limpopo Belt (from 200 to 300 km thick). Curiously, surface elevation decreases monotonically with increasing lithospheric thickness. This demonstrates the effect of the deep lithosphere on topography and gives us new information on the composition of the deepest parts of lithosphere.

1. Introduction

Cratons, the ancient cores of continents, preserve a long record of the evolution of the Earth. Observations from cratonic mantle xenoliths suggest that the process of the formation of cratons, dating back to the Archean Eon over 2.5 billion years ago, involved very high degrees of melt extraction (>40%) (Boyd et al., 1997; Boyd & Mertzman, 1987; Carlson et al., 2000; Pearson et al., 1995; Kamber, 2015; Walter, 1998) and produced mantle roots that remained attached to the overlying crust since the time of its formation (Carlson et al., 1999; Griffin et al., 2004; Pearson et al. 1995). The high degree and broad depth range of the melting explain the formation of the thick and severely depleted mantle lithosphere, buoyant and preserved over geologically long time. The existence of thick (at least 200 km), cold lithosphere beneath cratons today is

evident from the high-velocity anomalies beneath them revealed by seismic imaging (e.g., Grand & Helmberger, 1984; Gung et al., 2003; Jordan, 1975, 1988; Schaeffer & Lebedev, 2015), and diamond inclusions in kimberlites evidence its existence in the past, at the times of their eruption (Boyd et al., 1985), but the mechanisms of the formation of cratons, as well as how cratonic lithospheres evolve with time, remain a subject of debate.

The study of the seismic properties of the cratonic lithosphere yields essential constraints on the thermochemical structure of cratons and provides inferences on how they formed and evolved. Temperature has the strongest effect on seismic velocities, and the occurrence of anomalously high shear-wave velocities exceeding 4.7 km/s at 100–150 km beneath cratons is primary evidence for their lithosphere being cold and thick at present. The mineral composition of the Earth's crust and upper mantle also has a strong effect on seismic velocities—and, thus, can be inferred from seismic observations. For example, an increase in V_s below the crust-mantle interface (Moho) has been observed beneath stable continents in many seismic studies (e.g., Bruneton et al., 2004; Fishwick & Reading, 2008; Gaherty & Jordan, 1995; Lebedev et al., 2009; Lebedev & Van Der Hilst, 2008; Pedersen et al., 2009). It is a feature of the cratonic lithosphere that cannot be explained by a realistic geotherm (characterized, with rare exceptions, by temperature increasing with depth). It reflects, instead, composition and phase changes within the lithosphere (Hales, 1969; Lebedev et al., 2009). The width and slope of this positive V_s gradient can offer insights into the depth extent of the spinel-garnet stability field and on the abundance of garnet at depth.

The thickness of the cratonic lithosphere—or the depth of the lithosphere-asthenosphere boundary (LAB)—is its important basic property. The LAB is where the conductive lithospheric geotherm meets the mantle adiabat, so that the deeper it is, the colder the entire lithosphere is. The LAB depth and its lateral variations beneath cratons also contain information on the initial formation of the craton, on the depth range of the pervasive, crust-forming melting, and on the subsequent evolution and possible thinning of the lithosphere due to its interactions with the convecting mantle beneath (e.g., Griffin et al., 2003; Meier et al., 2016; Sobolev et al., 2011). The top of a low-velocity zone indicative of the warm sublithospheric mantle can be used to identify the lithosphere-asthenosphere boundary region (e.g., Eaton et al., 2009). The determination of the thickness of the cratonic lithosphere has proven challenging, however, because the amplitude of the low-velocity zone varies from one craton to another, and it is not even observed everywhere (Hansen et al., 2009; James et al., 2001; Larson et al., 2006; Lebedev & van der Hilst, 2008; Wittlinger & Farra, 2007).

The density of the mantle lithosphere has a profound effect on topography (e.g., Fullea et al., 2012; Vozar et al., 2014). In cratons, the negative buoyancy due to the low temperatures of the cold lithospheric lid is compensated, approximately, by the positive buoyancy generated by the depletion (Jordan, 1975). The composition and thickness of the cratonic mantle lithosphere are, therefore, two key factors that contribute to topography. Southern Africa has anomalously high topography on the large regional scale (Figure 1). Its mechanisms are a matter of debate. The notion of the African Superswell (Lithgow-Bertelloni & Silver, 1998; Nyblade & Robinson, 1994) was introduced to suggest a common origin for the high topography of the southern part of the African continent, the shallower bathymetry of the southeastern compared to southwestern Atlantic Ocean and the shallow bathymetry just east of southern Africa. Anomalously low seismic velocities in a large region of the lower mantle beneath southern Africa—a consensus feature of whole-mantle tomographic models (e.g., French & Romanowicz, 2015; Ritsema et al., 1999; Romanowicz & Gung, 2002; van der Hilst et al., 1997)—may indicate a broad, hot upwelling. Either such lower-mantle upwelling or hot material in shallower, sublithospheric mantle may give rise to dynamic topography across the entire region (e.g., Flament et al., 2014; Gurnis et al., 2000; Hager et al., 1985; Lithgow-Bertelloni & Silver, 1998).

The asymmetry in the southern Atlantic, however, appears to be primarily due to the southwestern Atlantic being anomalously deep, whereas the southeastern Atlantic adjacent to Africa has normal bathymetry for its seafloor age if volcanic ridges with thick crust are excluded (Müller et al., 2008, their Figure 11), at least according to some widely used plate cooling models (Stein & Stein, 1992). To the east of southern Africa, anomalously shallow bathymetry also coincides with what appears to be anomalous, probably thickened, crust (Müller et al., 2008). This leaves the high topography of the southern part of the African continent as the most clearly anomalous. Yet, relatively high elevation is not unusual for cratons and can also be seen in eastern South America, in East Siberian Craton and elsewhere.

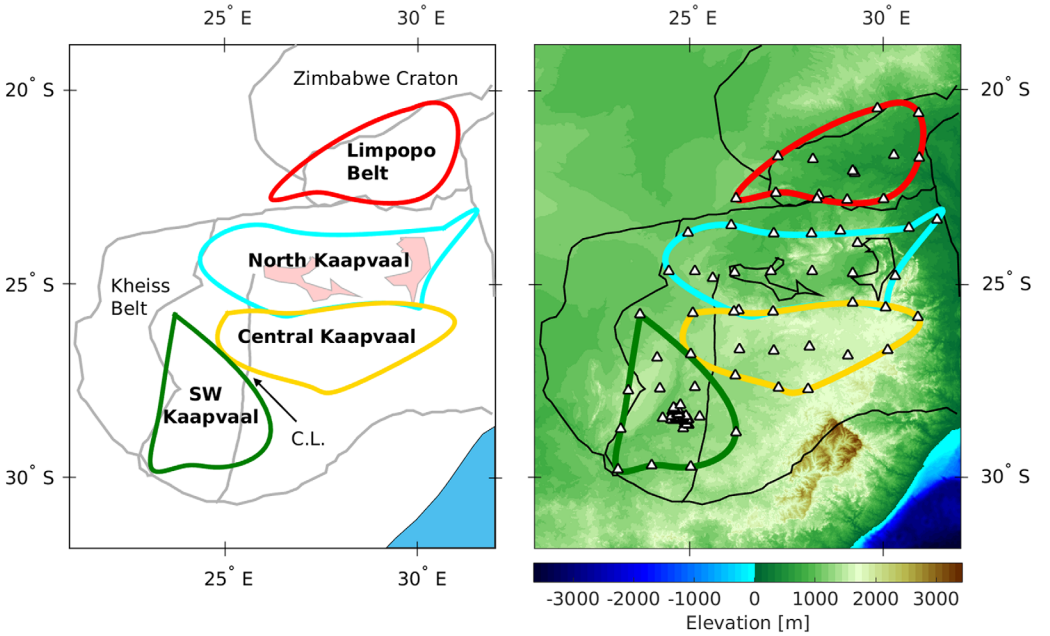

Figure 1. Tectonic setting and broadband seismic station coverage of southern Africa. (left) Main tectonic units and the four subregions (labeled in bold) considered in our study. (right) Topographic map of the region of study showing the location of the seismic stations (triangles), deployed mostly by SASE, and the four subregions, indicated with thick lines.

The strong effect of the thickness and density of the crust on surface topography means that relatively small variations in these parameters—within the uncertainties of our knowledge of them—will translate into hundreds of meters added to or subtracted from the calculated surface elevation (Fullea et al., 2011, their Table 5). For this reason, available data relating to southern Africa's lithospheric structure could be fit, in different studies, with models either with or without dynamic topography (e.g., Fullea et al., 2011; Jones et al., 2017; Artemieva & Vinnik, 2016; Muller et al., 2013), and the uncertainty over the drivers of the topography remains. It is thus important to improve our understanding of how the topography is affected by the lithospheric structure in southern Africa.

Surface waves are particularly sensitive to the shear-velocity structure of the lithosphere. Accurate Rayleigh-wave and Love-wave interstation phase-velocity measurements over broad period ranges enable one to determine the shear-velocity structure from the crust down to the deep asthenosphere (Lebedev et al., 2006, 2009; Meier et al., 2004; Soomro et al., 2016). Rayleigh and Love waves are sensitive to vertically and horizontally polarized shear velocities, respectively. The joint inversion of Rayleigh and Love phase velocities can resolve the radial anisotropy of shear velocities (defined as the difference between horizontally and vertically polarized shear speeds) and the isotropic-average shear velocities, at global and regional scales (Agius & Lebedev, 2013, 2014; Chang et al., 2014, 2015; Endrun et al., 2008; Ferreira et al., 2010; Khan et al., 2013; Lebedev et al., 2006; Nettles & Dziewoński, 2008; Visser et al., 2008). Radial anisotropy is important, first of all, because we must account for it in order to isolate the isotropic-average velocities, which can be related to temperature and composition. Anisotropy itself is also of interest, as it reflects anisotropic fabric of the rocks at depth and provides evidence on the past and current deformation. Beneath cratons, positive radial anisotropy in the lower crust and mantle lithosphere, indicative of horizontally oriented fabric ($V_{sh} > V_{sv}$), has been reported in a number of studies (Beghein & Trampert, 2003, 2004; Gaherty & Jordan, 1995; Gung et al., 2003; Khan et al., 2013; Lebedev et al., 2009; Moschetti et al., 2010; Nettles & Dziewoński, 2008). In the upper crust, the detection of radial anisotropy is often hindered by the lack of short-period surface-wave data.

In southern Africa, radial anisotropy has been detected in previous surface-wave studies (Adam, 2013; Freybourger et al., 2001; Saltzer, 2002), with horizontally polarized shear waves traveling faster than vertically polarized ones by a few percent. However, the depth profiles and lateral variations of anisotropy remain uncertain.

The shear-velocity models of the region, constrained by surface waves, also show a broad range of values, especially for the deep lithosphere (e.g., Adams & Nyblade, 2011; Bloch et al., 1969; Chevrot & Zhao, 2007; Freybourger et al., 2001; Larson et al., 2006; Li & Burke, 2006; Priestley, 1999; Priestley et al., 2006; Qiu et al., 1996; Saltzer, 2002; Yang et al., 2008). Seemingly contradictory results emerge when surface-wave and body-wave tomography models (Fouch et al., 2004; James et al., 2001; Zhao et al., 1999) are compared. Pronounced high-velocity anomalies extend below ~300 km depth in body-wave images but are confined to shallower depths (~200 km) in surface-wave models, prompting different lithospheric thickness estimates in the two types of studies. As shown by Priestley and Tilmann (2009), a bias toward overly deep high-velocity anomalies in body-wave tomography can result from vertical smearing, due to the limited depth resolution by the near-vertically traveling teleseismic body waves. While body waves can provide high lateral resolution beneath a dense array, it is surface waves that generally offer greater vertical resolution in the lithosphere-asthenosphere depth range.

In this study, we use accurate, broadband Rayleigh and Love fundamental mode phase velocities measured recently for the Kaapvaal Craton and Limpopo Belt (Adam & Lebedev, 2012). We invert the data for isotropic-average shear-wave velocity and radial anisotropy profiles beneath four subregions of the Archean southern Africa, with resolution from the upper-crust down to the asthenosphere. Our probabilistic inversion technique is based on a Markov chain Monte Carlo algorithm and uses exact, numerical solutions of the forward problem and the direct sampling of the parameter space (Ravenna & Lebedev, 2018). The Bayesian approach provides a way to quantify model nonuniqueness by generating an ensemble of accepted models that reflects the posterior probability distribution. Our results offer new insights into the architecture of the cratonic lithosphere of southern Africa, reveal pronounced lateral variability in the crustal and mantle structure, and indicate that lateral variations in the surface elevation within southern Africa are due, at least in part, to variations in the lithospheric thickness.

2. Data

Our data set includes Rayleigh and Love fundamental mode phase velocities measured by Adam and Lebedev (2012) using teleseismic seismograms at two permanent stations, BOSA and LBTB, and 112 temporary southern Africa Seismic Experiment (SASE; Carlson et al., 1996) stations in southern Africa (Figure 1). The Rayleigh-wave and Love-wave dispersion curves for various pairs of stations were obtained using a combination of the cross-correlation technique (Meier et al., 2004) and the automated multimode inversion (AMI) of surface and S waveforms (Lebedev et al., 2005), by simple averaging of the measurements at each station pair. The interstation dispersion curves of the fundamental modes were determined, with these two techniques, from the displacement field of events recorded at pairs of stations aligned approximately along the same great-circle path with an earthquake (within 10°). The higher-mode results of the AMI inversion were not considered in the computation of the average phase-velocity curves between station pairs.

The subsequent averaging over the hundreds of curves measured within the four subregions of southern Africa (Figure 1) produced robust average phase-velocity curves for each subregion (Adam & Lebedev, 2012): the Limpopo Belt and the northern, central, and southwestern Kaapvaal Craton. Each region is characterized by relatively uniform values of isotropic phase velocities over a broad period range and relatively uniform topography, crustal thickness, and the crustal V_P/V_S ratio (Nair et al., 2006; Nguuri et al., 2001; Yang et al., 2008; Youssof et al., 2013).

Removing the longest-period parts of the average dispersion curves (which were the least accurate, based on the criterion of curve smoothness), we obtained the curves to use in our inversions. Their period ranges are from 5 to 200 s for Rayleigh waves for all subregions, from 5 to 150–200 s for Love waves in three out of four regions, and from 5 to 50 s for Love waves in the central Kaapvaal region (Figure 2).

In most of the total period range (5–200 s), the phase velocities exceed those computed for the global reference model AK135 (Kennett et al., 1995) by 3–5%, indicating that shear velocities in both the crust and mantle lithosphere of the cratons are consistently higher than in younger continental lithospheres. The smallest phase-velocity anomalies (<3% around 20 s periods, Figure 2b) are where Rayleigh waves are sensitive to the Moho depth. The Moho depth is 7–10 km greater beneath the Limpopo Belt and northern Kaapvaal than in AK135 (e.g., Adam, 2013; Lebedev et al., 2013; Nair et al., 2006; Youssof et al., 2013). This lowers the

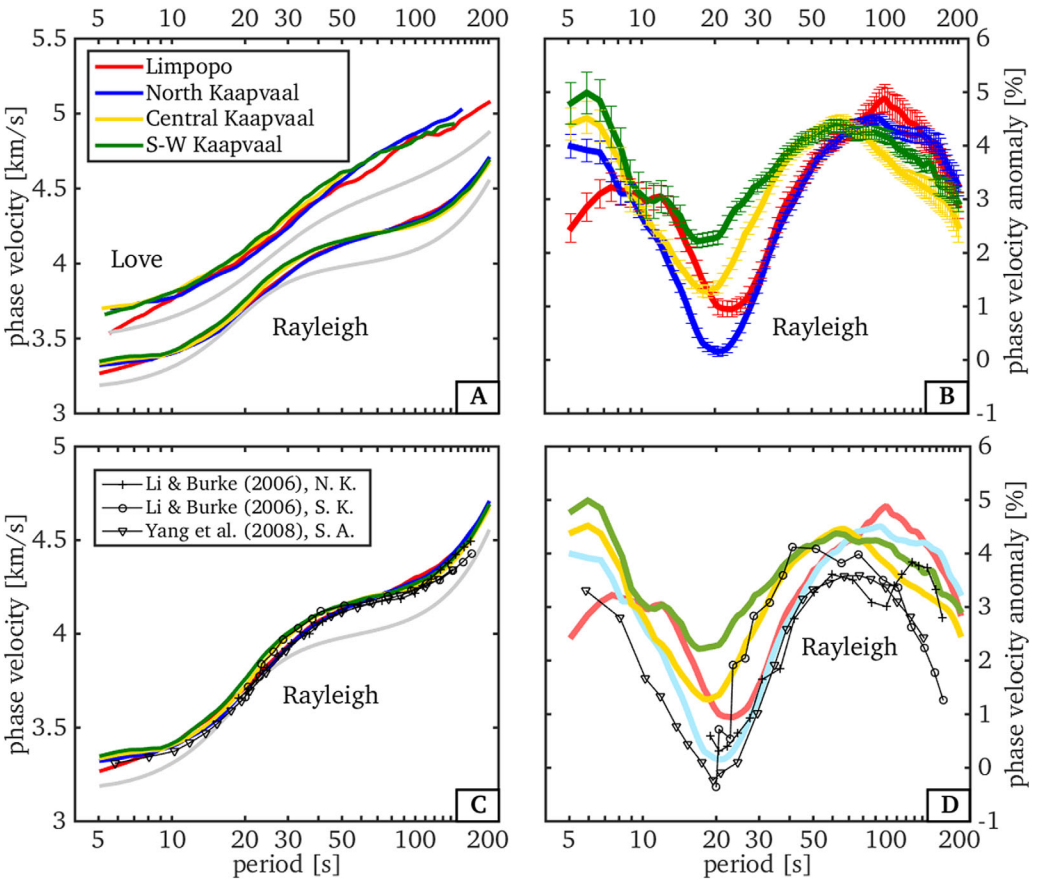

Figure 2. Subregion average dispersion curves measured by Adam and Lebedev (2012). (a) Rayleigh-wave and Love-wave dispersion curves for the four subregions, each computed by averaging over hundreds of interstation measurements. (b) Rayleigh-wave dispersion curves, as in Figure 2a, presented as anomaly with respect to AK135. The error bars indicate the data error estimated in this study, as shown in Figure 3. The same curves but without error bars are plotted below in Figure 2d. (c) Rayleigh-wave dispersion curves, as in Figure 2a, compared to those from previous studies for the north Kaapvaal region (Li & Burke, 2006), the south Kaapvaal region (Li & Burke, 2006), and the broader southern Africa region, including noncratonic areas (Yang et al., 2008). (d) Same data as in Figure 2c, but presented as anomalies with respect to AK135.

phase velocities and partially cancels the positive phase-velocity anomaly due to the high V_s in the cratonic lithosphere.

3. Inversion and Results

Our Bayesian inversion provides probabilistic ensembles of models for the radially anisotropic structure of the crust and upper mantle. This implementation of the Markov chain Monte Carlo sampling algorithm, developed and tested by Ravenna and Lebedev (2018), inverts Rayleigh and Love phase-velocity curves for the depth distribution of the radial shear-wave anisotropy and the isotropic-average shear velocity (V_s). The method avoids linear approximations of the relation linking surface-wave phase velocities to the shear-wave isotropic and anisotropic parameters, using exact numerical solutions. Importantly, it provides a way to address and quantify the nonuniqueness of solutions by the direct sampling of the parameter space.

In the McMC inversions in this study, uncorrelated noise on the observed phase velocities has been assumed, yielding a diagonal covariance matrix of data errors (Ravenna & Lebedev, 2018). The accurate estimation of measurement errors is important but notoriously difficult. The standard statistical estimates of the standard error yield very small values (much less than 0.1%), reflecting the very large numbers of measurements (on the order of 1,000 for each subregion). Jackknife or bootstrap resampling yields remarkably similar, small values, confirming the consistency of the statistics behind all these methods (Adam & Lebedev, 2012). These

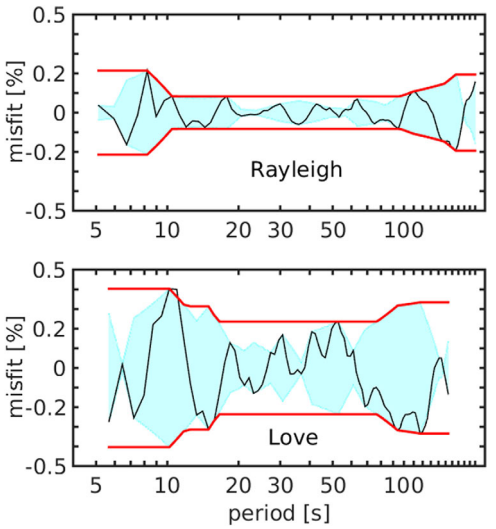

Figure 3. Estimates of data errors for the Rayleigh and Love phase-velocity curves of the North Kaapvaal region. The estimates (red lines) are derived from the envelope (pale blue bands) of the phase velocity misfit between the observed phase velocities and the phase velocities computed for the best-fitting model (black lines), yielded by a weakly regularized, gradient-search inversion of the data.

small values, however, are underestimates, because the methods assume that measurement errors are random, whereas actual measurements have both random and systematic errors (for example, diffraction or mode interference effects can be similar for measurements using earthquakes in the same source region).

The approach we use for error estimation is based on the fact that a dispersion curve for any Earth model is smooth, because the sensitivity of surface waves to Earth structure changes gradually (smoothly) with period. Using a gradient-search inversion with very weak regularization (just enough to ensure convergence), we typically find a best-fitting Earth model that we would not consider realistic. No matter how unrealistic the model, however, the dispersion curve computed for it is always smooth. The misfit between the data and the best-fitting smooth model thus quantifies the roughness of the measured curve that comes from errors in the measurements. (It is important to note that the misfit from a strongly regularized inversion would combine the effects of the errors and of a priori preferences for the type of acceptable model; in order to avoid this, regularization must be very weak.) Based on the misfit, which quantifies the frequency-dependent, error-caused roughness, we then obtain a conservative estimate of the frequency-dependent measurement error by interpolating between the maxima of the misfit envelope (red line in Figure 3 and supporting information Figure S1).

Following this rationale, the estimated errors on the Rayleigh and Love phase-velocity curves were determined after performing very weakly regularized, Levenberg-Marquardt gradient-search inversions (Agius & Lebedev, 2013, 2014; Lebedev et al., 2006; Meier et al., 2004; Ravenna & Lebedev, 2018) and evaluating the difference between the phase velocities computed for the best-fitting models and the phase velocities observed (Ravenna & Lebedev, 2018). The resulting error estimates for the North Kaapvaal region are shown in Figure 3. The errors (red lines) are estimated from the envelope of the phase-velocity misfit. They are just below 0.1% at 10–100 s periods for Rayleigh waves, increasing to up to 0.2% at the shortest ($<$10 s) and longest ($>$100 s) periods, and around 0.25% at 15–80 s for Love waves, increasing to up to 0.3–0.4% at the shortest ($<$15 s) and longest ($>$80 s) periods. The error curves for the other regions are estimated in the same way and are shown in supporting information (Figure S1).

The parameterization of the 1-D profiles includes isotropic and anisotropic model parameters and uses three crustal layers with constant elastic properties within each and 11 control points of spline polynomials in the mantle, down to the 410 km discontinuity. We also vary the values of the parameters at the 410 and 660 km discontinuities, and interpolate linearly between them; below 660 km the model is the isotropic AK135. The *a priori* information on the model parameters is expressed in terms of Gaussian prior probability distributions centered at reference velocity models with standard deviations of ~400 m/s (Bonadio et al., 2018; Ravenna & Lebedev, 2018). The reference model for V_s is AK135 in the mantle and CRUST 2.0 (Bassin et al., 2000) in the crust (Figure 4, black lines). The average crustal V_P/V_S for the four regions has been derived from Nair et al. (2006), and set equal to 1.74 for Limpopo Belt, 1.82 for North Kaapvaal, 1.7 for central Kaapvaal, and 1.72 for southwest Kaapvaal. The Moho depth is also a parameter of the inversion, constrained by a Gaussian prior distribution with a standard deviation of 3 km, centered at a reference value taken from Yang et al. (2008): 43 km for the Limpopo Belt and North Kaapvaal regions, and 36 km for central Kapvaal and southwest Kaapvaal. For the radial anisotropy parameters, a Gaussian prior distribution at each depth is centered at 0.

Figure 4 shows the depth distributions of the isotropic average V_s (left) and radial anisotropy (right) resulting from the inversions for the four subregions. The isotropic-average V_s is defined as the Voigt isotropic average, $V_S = \frac{2*V_{Sv}+V_{Sh}}{3}$, and radial anisotropy as $R = \frac{V_{Sh}-V_{Sv}}{V_S}$, where V_{Sv} and V_{Sh} are the vertically and horizontally polarized shear velocities, respectively.

The synthetic phase velocities corresponding to the models of the posterior distribution for the North Kaapvaal region are shown in Figure 5 (left), and for the other regions in supporting information (Figures S2–S4).

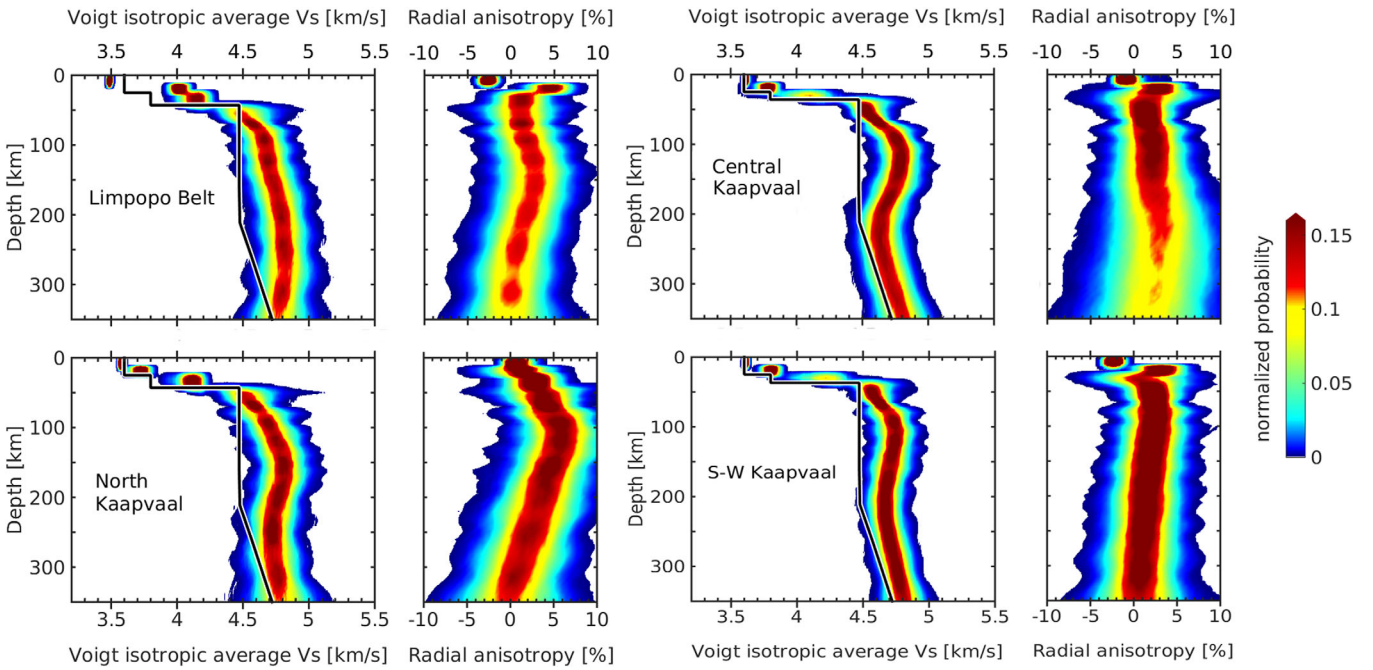

Figure 4. Marginal posterior probability distributions for V_s and radial anisotropy resulting from the inversions of the Rayleigh and Love phase-velocity curves for each of the four subregions. The yellow contour boundaries correspond to one standard deviation of the sampled distributions. The isotropic reference model AK135 (Kennett et al., 1995) is plotted with solid black lines.

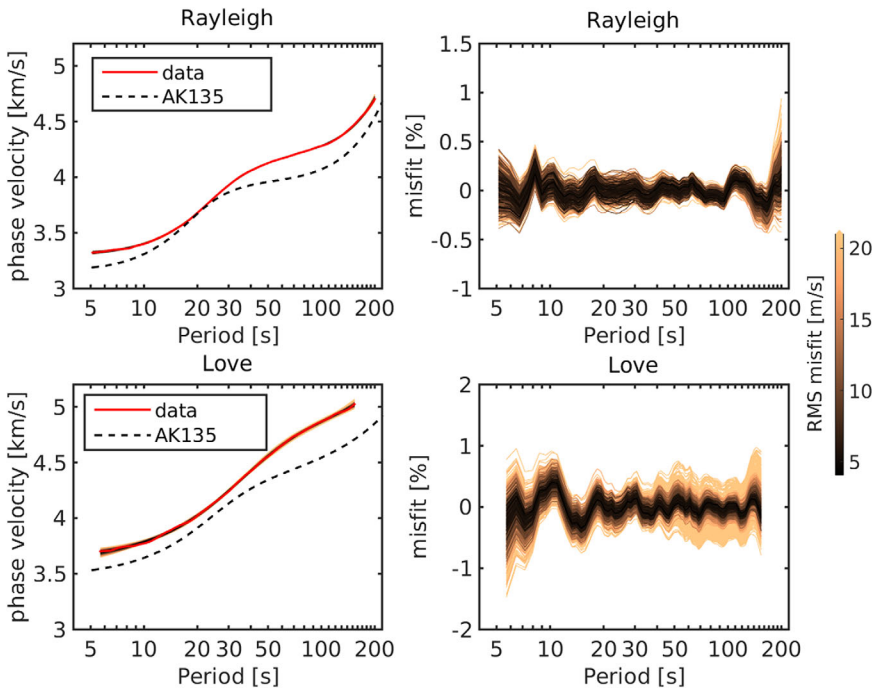

Figure 5. (left) Rayleigh (top) and Love (bottom) phase-velocity curves measured (red lines) and computed (black to bright copper lines) in the inversion for radial anisotropy in the north Kaapvaal region. The phase velocities computed for the model AK135 are plotted as black dashed lines. (right) The misfits yielded by the Rayleigh (top) and Love (bottom) synthetic phase velocities as in panels on the left, computed as synthetic minus data. Each bundle of (left) computed curves and (right) misfits is a representative subset (1,000 profiles) of the (post burn-in) computed phase velocities, which includes the worst-fitting and the best-fitting curve.

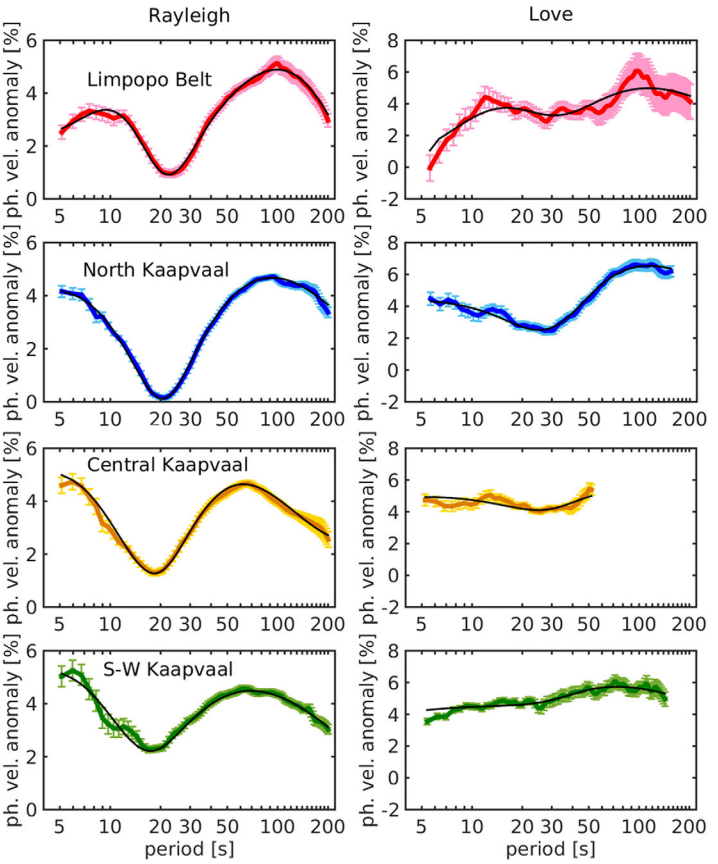

Figure 6. Rayleigh and Love phase-velocity anomalies with respect to AK135, observed (thick colored lines) and computed (thin black lines) for the mean models of the McMC posterior distributions for the four subregions in southern Africa. The plotted error bars indicate the data error estimated as shown in Figure 3.

The mean models of the posterior distributions fit the data closely, within a small portion of percent in most cases (Figure 6). The Love-wave data for the Limpopo and central Kaapvaal regions show more random noise than the Rayleigh-wave data, but the oscillatory random noise is not expected to bias the solutions significantly (e.g., Bartzsch et al., 2011; Lebedev et al., 2013).

Plotting the mean models of the posterior distributions in Figure 7, we note, first, the very high velocities at 100–150 km depths, up to 4.7–4.8 in all subregions. These values fall near the highest-velocity values within the range reported for cratons globally (Hirsch et al., 2015; Lebedev et al., 2009; Pedersen et al., 2009; Schaeffer & Lebedev, 2015). Another robust feature in all regions is the positive velocity gradient (V_s increase with depth) from the Moho to ~100–150 km depth. In the Limpopo region, the increase continues down to ~200 km. Around 200 km, the central and southwestern regions show V_s anomalies decreasing, consistent with temperature anomalies decreasing near the LAB at this depth. In northern Kaapvaal and, especially, Limpopo, a pronounced high-velocity anomaly extends deeper, down to depths as great as ~300 km, with velocities in the 200–300 km depth range 3–6% higher than average.

A comparison of our V_{Sv} posterior distributions with V_{Sv} profiles from previous surface-wave studies in South Africa (Adams & Nyblade, 2011; Li & Burke, 2006; Priestley, 1999; Yang et al., 2008) is shown in Figure 8. In the shallow upper mantle just below the Moho, the positive velocity gradient is present in all profiles but one, for all parts of southern Africa. The profiles of Yang et al. (2008) are constrained by dispersion curves that are very smooth, similarly to ours, which is indicative of small errors. The V_S profiles of Yang et al. (2008), from the Moho to their maximum depths, are consistent with ours both beneath the Limpopo Belt and central

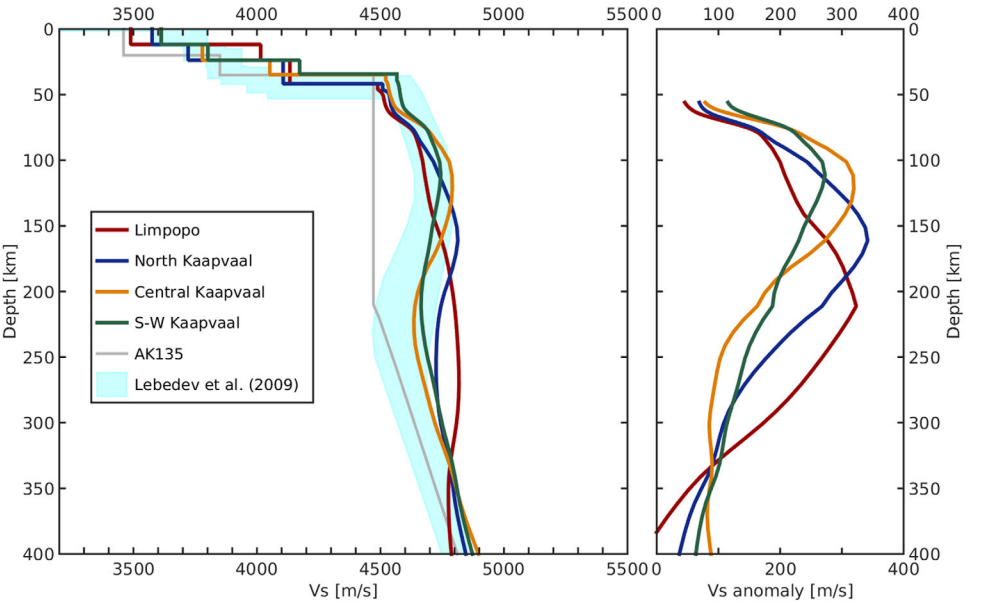

Figure 7. (left) V_S isotropic-average depth profiles beneath the four subregions in southern Africa. Colored lines show the mean models of the McMC posterior distributions. The pale blue band indicates the range of V_s models for various cratons computed by Lebedev et al. (2009). (right) V_s anomalies in the mantle beneath the four subregions relative to AK135.

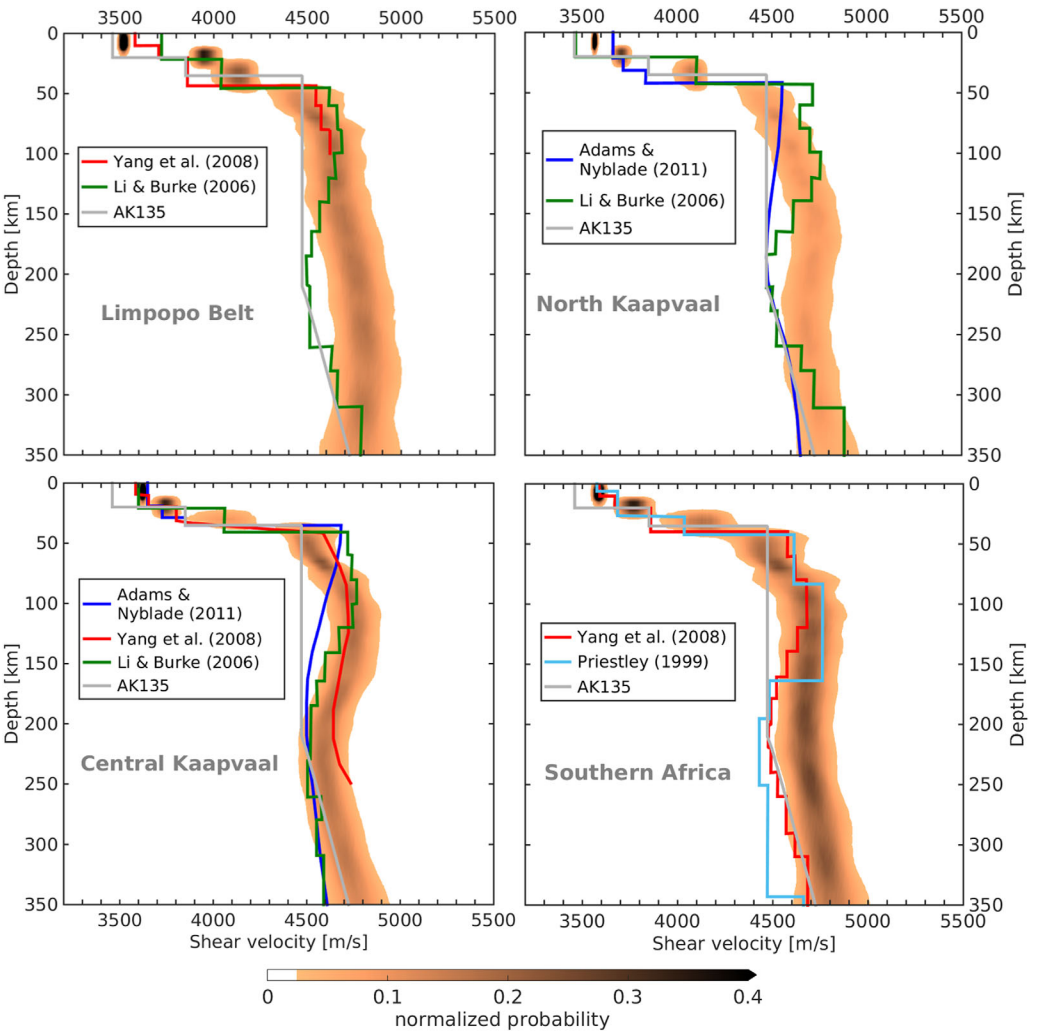

Figure 8. Comparison between the V_{Sv} posterior distributions obtained in this study (bright to black copper color scale) and the previously published models from Yang et al. (2008) (red), Li and Burke (2006) (green), Adams and Nyblade (2011) (dark blue), and Priestley (1999) (light blue) in the different subregions and beneath the entire region. The gray line shows AK135 for reference.

Kaapvaal. For the southern Africa average, Yang et al. (2008) included both cratonic and noncratonic parts of the region, whereas our average is over cratons only. We thus see an expected difference between the profiles, with the one from Yang et al. (2008) slower.

The phase-velocity curves of Li and Burke (2006) are substantially less smooth, compared to ours or those from Yang et al. (2008) (Figure 2), which is an indication of larger errors. For example, the jump in phase velocity of nearly 1% between 100 and 116 s cannot be explained by any realistic Earth structure and indicates noise, the amplitude of which is as high as the differences between phase velocities in the different subregion (Figure 2d). The noise in the data—comparable in amplitude to the subtle signal of deep lithospheric structure in phase velocities—can account for at least some of the substantial differences between some of the profiles published for southern Africa (Figure 8). This illustrates how phase-velocity measurements with errors well below 0.5% are required to resolve the structure of the lithosphere.

The posterior distributions of the sampled Moho depths (see supporting information Figure S5) show agreement with the a priori models, based on published values. For all regions, the distributions are centered at values at most $\pm$2 km different from the reference ones, confirming the presence of a thick crust beneath the North Kaapvaal and Limpopo Belt ($\sim$43 km), and a thinner crust beneath the central and southwestern

Kaapvaal regions (~36 km). We resolve positive radial anisotropy ($V_{sh} > V_{sv}$) in the midlower crust and upper mantle beneath all regions. In three regions out of four, anisotropy reaches 2–3%, similar to the global average PREM model (Dziewonski & Anderson, 1981). The North Kaapvaal region stands out and shows stronger radial anisotropy in the mantle, reaching ~5% near 100 km depth. The upper-crust depth range (0–13 km) is characterized, on average, by negative anisotropy ($V_{sh} < V_{sv}$) in two out of four regions (Figure 4). We attribute this to aligned cracks and microfractures in the uppermost 5 km of the crust, opened by the tectonic stress (e.g., Crampin, 1978; Nur, 1971). Radial anisotropy shall be discussed in more detail in a forthcoming publication, together with azimuthal anisotropy beneath southern Africa.

4. Discussion

4.1. Vs Increase With Depth Beneath the Moho: Evidence for Compositional and Phase Changes

A realistic geotherm, reasonably close to steady state, is characterized by an increase of temperature with depth within the mantle lithosphere. If the mantle rock is the same at different depths within the lithosphere, this implies a decrease in seismic velocities with depth (Shapiro & Ritzwoller, 2004a, 2004b). Therefore, the increase in V_s with depth displayed by our models (and those in previous studies) implies that the rock is not the same at different depths: it must undergo compositional changes, phase changes, or both (e.g., Begg et al., 2009; Deen et al., 2006; Griffin et al., 1999; Hales, 1969; Hieronymus & Goes, 2010; Lebedev et al., 2009). Because this V_s gradient is clearly not thermal in origin—and, thus, can be attributed entirely to the compositional and phase changes—its properties and lateral variations are, potentially, a valuable source of information on the composition and evolution of the lithosphere.

To verify the robustness of the V_S gradient in our models, we tested the influence of the crustal V_P/V_S ratio on it. V_P variations in the crust have an effect on Rayleigh phase speeds and can trade-off with the isotropic-average V_S or radial anisotropy in the uppermost mantle (e.g., Shapiro & Ritzwoller, 2002). We performed a series of gradient-search inversions with different values of the crustal V_P/V_S ratio in a very broad (1.6—1.9) range (Hacker et al., 2015). The results (Figure 9) confirm that the crustal V_P/V_S trades off with V_S in the uppermost mantle (lower V_P can compensate the effect of higher V_s, and vice versa). The maximum V_S just below the Moho, for a (very low) $V_P/V_S = 1.6$, is up to 2% higher than the V_S obtained with the crustal V_P/V_S used in our Monte Carlo inversions. Thus, even if V_P/V_S ratios were unusually small and we were assuming, mistakenly, normal crustal values, the resulting error could not account for the 3–7% increases in V_S between the Moho and 100–200 km, as seen in our models (Figure 7). Errors in assumed crustal V_P/V_S

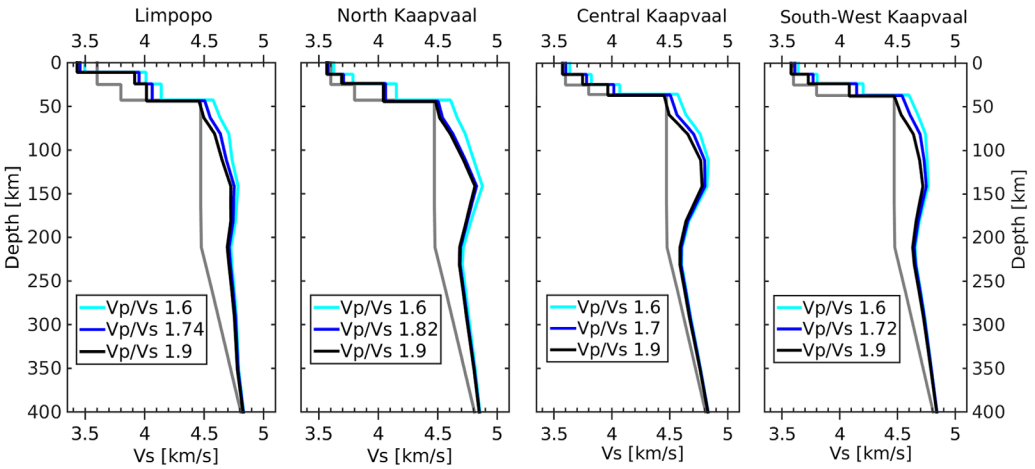

Figure 9. The influence of the V_p/V_s ratio in the crust on the gradient of the isotropic average V_s in the uppermost mantle. Gradient-search inversions of the Rayleigh and Love phase velocities from the four subregions were performed assuming different values of the crustal V_p/V_s (kept fixed during the inversions). The light blue lines show the best-fitting models obtained for an unrealistically low V_p/V_s, the black lines show the best-fitting models obtained for an unrealistically high V_p/V_s, and the blue lines show the best-fitting models obtained for the V_p/V_s consistent with published data and used in our Monte Carlo inversions. The increase of V_s with depth in the uppermost mantle beneath the Moho is robust; it is present even with a very low V_p/V_s ratio assumed.

ratios may affect the amplitude of the V_S increase in the uppermost mantle but cannot be the cause of this persistent feature of the models.

Shear velocities in the lower crust of our models are high, much higher than in CRUST2.0 for the locations or in AK135. This is required by the high phase velocities at short periods, sensitive to crustal structure (Figure 2). In order to test the effect of changing V_S in the lower crust on the upper mantle V_S, we performed a series of inversions. We could fit the data with lower crustal V_s, but this required models with oscillations in V_S and radial anisotropy and with Moho much shallower than reported for the regions. The effect on the V_S between the Moho and 100–150 km depth was small, and the positive V_s gradient below the Moho changed little (see supporting information Figure S6).

It has been proposed (Green & Hales, 1968; Hales, 1969; Revenaugh & Jordan, 1991) that the V_S increase with depth in the shallow lithosphere can be attributed to the phase change from spinel peridotite to garnet peridotite (the "Hales discontinuity" at ~80 km depth). This phase transition occurs at higher pressures and over a broader depth interval in the presence of chromium (Grütter et al., 2006; Klemme, 2004; Klemme et al., 2009). Hence, the very Cr-rich bulk compositions observed in xenoliths from kimberlites (Grütter et al., 2006; Kopylova & Caro, 2004; O'Reilly & Griffin, 2006) imply a phase transformation over a broad depth range, giving rise to a "Hales gradient" (Lebedev et al., 2009). Temperature also plays a role: in a hot lithosphere, the transition occurs across a narrow depth interval, whereas in a cold cratonic lithosphere, garnet, and spinel coexist over a wide range of pressures (i.e., depths) (Ziberna et al., 2013). In a relatively fertile cratonic mantle (containing garnet with lherzolitic major elements compositions) spinel can coexist with garnet to about 120 km depth, while in an ultradepleted harzburgitic mantle it can be stable at over 180 km depth (Ziberna et al., 2013).

It has also been suggested (e.g., Bruneton et al. 2004) that the presence of a very fertile composition at shallow depths in the lithosphere, such as clinopyroxene-rich cumulates or metasomatized peridotites may be responsible for the relatively low V_S in the uppermost mantle. Such anomalous, enriched compositions are unlikely to be as ubiquitous as the sub-Moho V_S increases beneath cratons, but they may play a role in lowering seismic wave speeds in the uppermost mantle at some locations, contributing to the lateral variability of the sub-Moho V_S gradient beneath cratons (e.g., Fishwick & Reading, 2008).

We argue that the emergence of garnet at 80–150 km depths provides the primary contribution to the observed V_S increase with depth. The presence of the aluminous phase (garnet) increases shear velocities (Faul & Jackson, 2005; Schutt & Lesher, 2010; Stixrude & Lithgow-Bertelloni, 2005). Even though there may be little spinel left in the highly depleted uppermost mantle of many cratons, which would reduce the impact of the spinel peridotite-garnet peridotite transformation itself, the appearance of garnet by means of exsolution from mantle orthopyroxene has been inferred in many studies, in particular in southern Africa (e.g., Bell et al., 2005; Simon et al., 2003; Tomlinson et al., 2017). The occurrence of the exsolution and the distribution of garnet depends on the cooling and metasomatic history of the lithosphere (e.g., Saltzer et al., 2001). Pressure and temperature estimates of Gibson (2017), obtained from the mantle xenoliths and megacrysts from the Kaapvaal Craton, revealed that the orthopyroxenes with exsolved garnet were entrained from a broad, 85–175 km depth interval. This roughly coincides with the depth range where cratonic lithosphere displays the highest seismic velocities, in most cases, in southern Africa and elsewhere. Gibson (2017) inferred that the garnet exsolution probably occurred during the lithospheric thickening, possibly during the Archean cratonization; further evidence is needed to establish the timing and mechanisms unambiguously. Seismic data relating to the amplitude and lateral variability of the sub-Moho increase in V_S with depth can help by providing new observational constraints on the composition, with broader inferences on the evolution of the cratons.

4.2. Vs in the Lithosphere: Inferences for Temperature and Composition

The high-velocity anomalies displayed by the V_s profiles of the four subregions (Figures 4 and 7) are indicative of a cold and thick cratonic lithosphere (Artemieva, 2009; James et al., 2001; Jordan, 1975). If inferred from the onset of the low-velocity zone, indicating temperature increase with depth combined with the transition from elastic to viscoelastic behavior (Faul & Jackson, 2005; Stixrude & Lithgow-Bertelloni, 2005), the thickness of the lithospheric lid appears to vary significantly between the four regions.

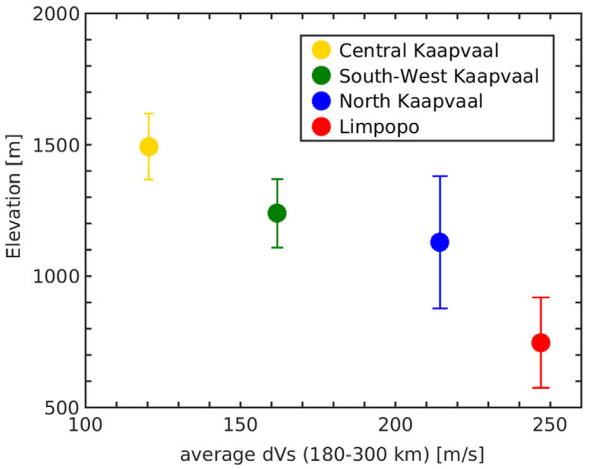

Figure 10. Correlation between the average elevation within a subregion and the average shear-velocity anomaly (with respect to AK135) in the 180–300 km depth range beneath it. Regions with higher velocities at 180–300 km (and, by inference, lower temperature in this depth range and, thus, thicker lithosphere) show lower elevations. The vertical bars indicate the standard deviations of the average elevations in each region.

The central and southwest Kaapvaal, mean V_s profiles (Figure 7) are similar in their entire depth range, suggesting similar upper mantle structure. The North Kaapvaal and Limpopo Belt profiles are distinctly different. Beneath the central and southwestern Kaapvaal Craton the increase in V_s reaches its peak at ~100 km depth, and the high-velocity anomaly is underlain by a zone with relatively low velocities, marking the bottom of the seismic lithosphere. A minimum V_s value (about 4.65 km/s, still above the global average) is reached at 200–250 km depths. Beneath the northern Kaapvaal and Limpopo Belt, in contrast, a low-velocity zone is not required by the data. In the North Kaapvaal mean profile, there is a slight decrease in V_s at 200–250 km; in Limpopo, high velocities extend down to ~300 km, suggesting the presence of a very thick lid.

Both temperature and composition must contribute to the observed patterns. In the uppermost mantle, the slope and width of the "Hales gradient" (Lebedev et al., 2009) are controlled by the composition of the lithosphere. A more depleted composition can broaden the depth range of the spinel-garnet phase transitions up to depths below 150 km, and the exsolution of garnet from mantle orthopyroxene can also increase V_s below 80 km depth. In the shallow mantle lithosphere, the lowest velocities are observed beneath the North Kaapvaal and, especially, the Limpopo Belt, suggesting less depleted compositions (possibly, affected by hydration and metasomatism) in the shallow mantle. An inference of more depleted lithosphere at 150–200 km depths and more fertile and melt-enriched lithosphere above ~100 km in the north, compared to the south, is consistent with the chemical profiles for the lithospheric mantle beneath southern Africa (Begg et al., 2009). A temperature increase with depth is probably the main cause for the onset of the low-velocity zone below ~200 km in some of the regions, with a maximum velocity reduction of ~3% in the central Kaapvaal. A more fertile mantle composition, or an increase in iron content, would not generally account for a shear-velocity reduction of a few percent (Lee, 2003; Schutt & Lesher, 2006, 2010), which is consistent, specifically, with xenoliths data from the Kaapvaal Craton (James et al., 2004).

The V_s anomaly beneath the Limpopo Belt can be explained by very thick cratonic lithosphere, with the LAB at ~300 km. It is possible, alternatively, that this thick layer of cold mantle comprises a thinner lithosphere of an Archean age and a fertile mantle layer beneath it that is anomalously cold but transient—cooled from above but likely to eventually drip into the deep mantle due to its lack of compositional buoyancy. Azimuthal seismic anisotropy, however, shows E-W oriented fabric beneath Limpopo from shallow mantle lithosphere down to ~300 km, around which depth the fast direction changes to NNE-SSW (Adam, 2013; Adam & Lebedev, 2012; Ravenna et al., 2017; Sodoudi et al., 2013), parallel to the absolute plate motion (Argus et al., 2011; Becker et al., 2015; Gripp & Gordon, 1990). This is consistent with frozen anisotropy in the entire 100–300 km depth range formed by the same deformation processes, before or during the Archean-Paleo-Proterozoic stabilization of the lithosphere (Holzer et al., 1998; Kamber et al., 1995). Taken together, the evidence from the isotropic average V_s and anisotropy suggests that the ancient cratonic root of the Limpopo Belt is, indeed, ~300 km thick.

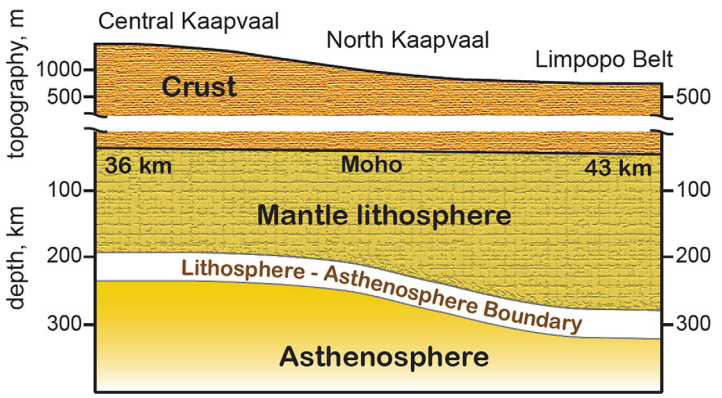

Figure 11. Schematic cross section from the central Kaapvaal Craton to the Limpopo Belt. The Moho depth values are subregion averages from published studies (Nair et al., 2006; Nguuri et al., 2001; Yang et al., 2008; Youssof et al., 2013). The LAB is as determined in this study. The south-to-north increase in the lithospheric thickness coincides with a decrease in the surface elevation.

4.3. Lithospheric Architecture and Topography

The variations in the lithospheric thickness revealed by our models show a striking anticorrelation with the surface elevation (Figure 10).

Regions with lower velocities in the 180–300 km depth range, and thus with a thinner lithosphere (central and southwest Kaapvaal), exhibit higher topography, whereas the regions with higher velocities and thicker lithosphere (North Kaapvaal and Limpopo Belt)—lower topography (Figure 11). This pattern can be used to estimate the composition of the deepest lithosphere we have detected.

The south-to-north decrease in the surface elevation is not due to a crustal thickness decrease: the crust, on the contrary, thickens from ~36 km beneath central and SW Kaapvaal to ~43 km beneath northern Kaapvaal and Limpopo. The density of the crust, however, also has a strong effect on topography, and this needs to be estimated so as to isolate the effect of the lithospheric thickness.

In order to estimate the effect of the crust on topography, we used the integrated petrological-geophysical modeling tool Litmod (Afonso et al., 2008; Fullea et al., 2009) and computed the surface elevation for a series of isostatic thermochemical models of the lithosphere. Figure 12 (left) shows the relationship between the average crustal density and the predicted isostatic topography. The mantle chemical stratification is fixed and taken from Fullea et al. (2011), who based it on xenolith data. The model of Fullea et al. (2011) (green square) is for the west-central Kaapvaal Craton, with a Moho depth of 35 km and an average crustal density of 2,820 kg/m^3, based on data from regional crustal studies. The model is isostatic (no dynamic topography) and reproduces the observed topography of 1.2 km.

In the Limpopo Belt and northern Kaapvaal regions, the lower crust is likely to be denser, probably affected by underplating during the Phanerozoic Karoo as well as earlier magmatism (Cox, 1992; De Wit, 1998; Eales et al., 1984; Hofmann et al., 1998; Holzer et al., 1998). This is consistent with the results of seismic (Durrheim & Mooney, 1991; Gore et al., 2009) and gravity studies (Gwavava et al., 1992), suggesting the presence of more mafic lower crust compositions beneath the Limpopo Belt and northern Kaapvaal, compared to the central Kaapvaal Craton. Assuming the velocity-density relationships of Christensen and Mooney (1995) and their values for the middle of the range of compressional-wave crustal velocities in ancient orogens (with crustal thickness $>$ 40 km), we estimated an average crustal density of $2,930 \pm 30$ kg/m^3 for the Limpopo region.

Considering the 2,900–2,960 kg/m^3 range and drawing a straight line through the red triangles in Figure 12 (right; dashed red line), we estimate that the change of the crustal density alone—from the central Kaapvaal Craton to the Limpopo Belt—can produce a 0 to +800 m elevation change, assuming a 45 km Moho depth for Limpopo. Similarly, assuming a 42 km Moho depth for Limpopo, the estimated elevation change is −500 to +300 m. The combination of the two ranges (Moho depth 42–45 km, density 2,900–2,960 kg/m^3)

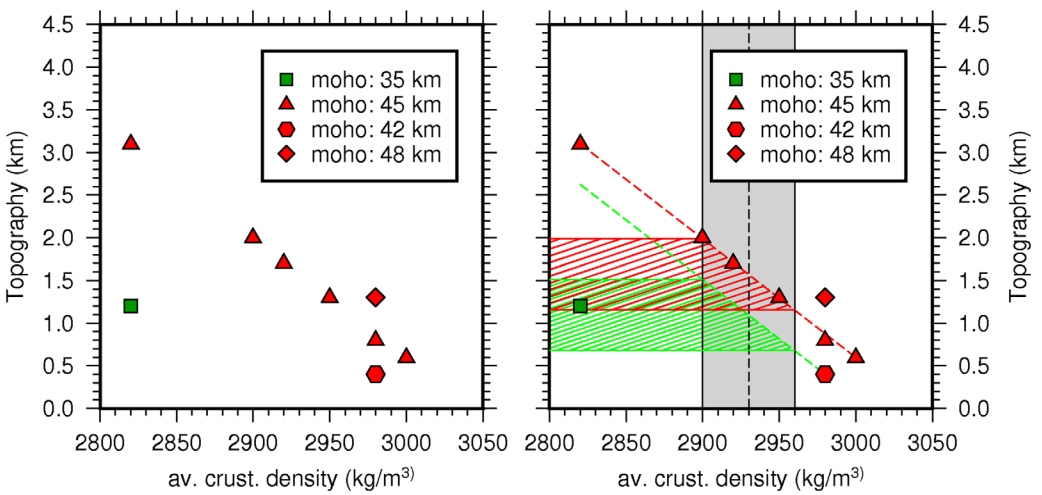

Figure 12. (left) The effect of the average crustal density on topography. The mantle composition is fixed, taken from Fullea et al. (2011). The model of Fullea et al. (2011) (green square) was constructed for west-central Kaapvaal Craton and included a 35 km crust with relatively low density, based on regional crustal studies (Fullea et al., 2009, and references therein). Beneath the Limpopo Belt, the crust is around 42–45 km thick (Nair et al., 2006; Nguuri et al., 2001; Yang et al., 2008; Youssof et al., 2013). Red triangles show the surface elevation as a function of the average crustal density, assuming a 45 km thick crust, and the diamond and octagon show the effect of a 3 km change in the crustal thickness. The 3 km increase in the crustal thickness has a somewhat greater effect because the thicker crust has more radioactive heat production and makes the lithospheric geotherm warmer, which increases the surface elevation. (right) Estimation of the elevation change produced by changes in crustal density and crustal thickness. For a 45 km Moho depth, the inferred elevation change is indicated by the red shaded area, whereas for a 42 km Moho depth the inferred change in topography is represented by the green shaded area.

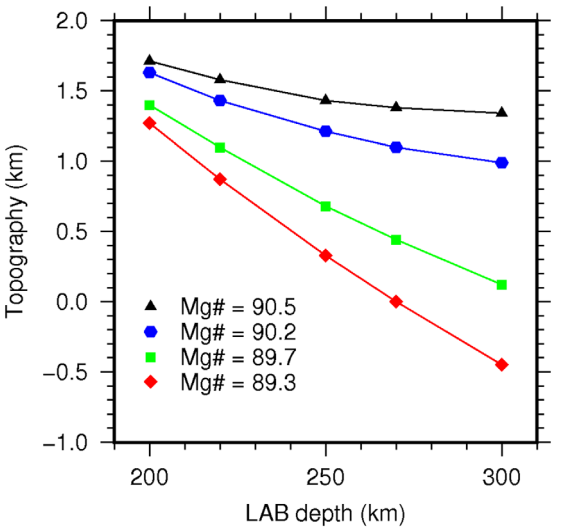

Figure 13. The effects of the lithospheric thickness and the composition of the lower lithosphere on topography. The composition above 165 km is fixed, taken from Fullea et al. (2011). The surface elevation was calculated for different thicknesses and compositions of the layer between 165 km and the LAB depths, the compositions ranging from fertile (Mg# 89.3, red diamonds) to slightly depleted (Mg# 89.7, green squares; Mg# 90.2, blue hexagons) to moderately depleted (Mg# 90.5, black triangles).

yields an estimate of the net elevation difference due to the crustal structure variations in the range of −500 to +800 m. The actual drop in the elevation from the central and southwestern Kaapvaal Craton to the Limpopo Belt is ∼750 and ∼500 m, respectively. Subtracting the crustal structure contribution from the actual elevation change, the effect of the lithospheric thickening on topography can be estimated at −250 to −1,550 m for a 750 m drop in elevation and at 0 to −1,300 m for a 500 m drop in elevation.

The net buoyancy of the cratonic mantle lithosphere is a sum of the negative buoyancy due to its low temperature and the positive buoyancy due to its depleted composition. If 100 km of highly depleted mantle is added at the bottom of a 200 km thick lithosphere, to make it 300 km thick, then the resulting change in surface elevation will be positive; if the extra lithosphere is weakly depleted, then it will be negative. In Figure 13, we plot calculated changes in topography for different total thicknesses of the lithosphere and for a range of compositions (from fertile to moderately depleted) of the part of the lithosphere below 165 km depth. The composition of the mantle above 165 km is kept constant, same as in Fullea et al. (2011); our choice of the 165 km compositional boundary is based on the model of Fullea et al. (2011). Adding 100 km of fertile lithosphere in the 200–300 km depth range (red diamonds) would decrease the elevation by over 1,700 m, a value outside the range allowed by the estimated uncertainty in the crustal structure. Slightly to moderately depleted compositions, with Mg# ranging from 89.7 (green squares) to 90.5 (black triangles), correspond to elevation drops in the range ∼1,300 to ∼350 m and are compatible with the observed topography and realistic variations in the crustal structure. A drop of ∼0 m (the lower limit of our estimated ranges, with the crustal contribution subtracted) can be explained by increasing the lithospheric thickness with a 100 km layer with Mg# around 90.8. Thus, given the Moho depth 42–45 km in the Limpopo Belt and 35–36 km in the southwestern-central Kaapvaal, given an estimated average density of the crust of the Limpopo Belt in the 2,900–2,960 kg/m^3 range, and given the lithospheric thickness change from 200 to 300 km, as suggested by our data, the possible range of compositions of the Limpopo lithosphere in the 200–300 depth range is characterized by Mg# 89.7–90.8.

That the Limpopo lithosphere below 200 km is depleted only a small amount is consistent with the chemical profiles based on xenolith data (Begg et al., 2009), which indicate melt-metasomatized rocks below 200–210 km. Between 110–120 and 200–210 km below Limpopo, the chemical profiles are dominated by highly depleted harzburgite and lherzolite.

This confirms that Limpopo's lithosphere in this depth range is likely to be at least as compositionally buoyant as that beneath central and southwestern Kaapvaal and that the lower topography in the Limpopo Belt is not due to higher lithospheric density at 100–200 km and, instead, has to be caused by the addition of weakly depleted lower lithosphere below 200 km.

The thickness of the lithosphere in central and southwestern Kaapvaal Craton, according to our results, is around 200–220 km. This is below the ∼260 km estimates based on mantle xenoliths (Fullea et al., 2011; Muller et al., 2013). The lithospheric thickness, however, can change with time. The lithosphere of cratons, in particular, can be thinned by thermochemical plumes from the deep mantle (Legendre et al., 2012, 2018; Sobolev et al., 2011). Thus, the same mantle plume that could have been the underlying cause of the eruption of the numerous kimberlites in central and southwestern Kaapvaal Craton may well have eroded the lithosphere there soon after the kimberlites erupted. A comparison of our results with inferences from the xenolith data suggests that this is, indeed, the case, with the lithosphere having thinned since having been sampled by the kimberlites.

The lithospheric density profiles corresponding to the steady state thermochemical models computed for each point in Figure 13 show jumps to higher values across the LAB (supporting information Figure S7). For a 300 km thick lithosphere and compositions in the 165–300 km depth range with Mg# 89.7 and Mg# 90.5,

the density jumps from the lithosphere to asthenosphere are 15.69 and 45.72 kg/m^3, respectively. The density contrasts are similar for LAB depths that deviate from 300 km. For example, for a 250 km thick lithosphere with the composition in the 165–250 km depth range with Mg# 89.7 or with Mg# 90.5, the density jumps are 15.85 or 48.18 kg/m^3, respectively. Even though the density difference is relatively small, the deep part of the thick lithosphere (in the 200–300 km depth range) does have compositional buoyancy, which must have facilitated its survival for a geologically long time, probably since the Archean-Palaeo-Proterozoic stabilization of the Limpopo Belt.

Our results reveal a relationship between regional variations of topography and lithospheric thickness. They are valid regardless of the presence or absence of dynamic topography, which, if caused by a deep mantle anomaly, would have a longer wavelength than these regional variations. Regarding dynamic topography itself, published estimates are, typically, a few hundred meters (e.g., Flament et al., 2014, and references therein). This is equal to or less than the change in elevation due to a crustal density change of only 50 kg/m^3 ($\sim$1.5%) (Figure 12). Given the uncertainties in our current knowledge of the average crustal densities, it is not surprising that thermochemical models both with and without dynamic topography have been found to fit available data (e.g., Fullea et al., 2011; Jones et al., 2017; Muller et al., 2013). Our new results on the variations in the thickness of southern Africa's lithosphere offer useful new information on the topography-lithospheric structure relationship. If the range of crustal densities that we used in our estimates can be narrowed down, this will provide, by means of the same reasoning as used above, a narrower range of values for the composition of the deep lower lithosphere beneath the Limpopo Belt.

5. Conclusions

Probabilistic inversions of our broadband dispersion curves from southern Africa offer new insights into the chemical and thermal structures of its ancient lithosphere. The V_s increase with depth in the shallow mantle lithosphere is a robust feature observed for all subregions. It can be explained primarily by the gradual emergence of garnet in the deeper lithosphere (>80 km depth), which results in a V_s increase. Garnet emerges due to the spinel peridotite-garnet peridotite phase transformation (Hales, 1969), spread over a broad depth interval in the presence of high bulk Cr/(Cr + Al) ratios in depleted lithospheric compositions (Klemme, 2004; Lebedev et al., 2009). Specifically, much of the garnet may appear by means of exsolution from mantle orthopyroxene, documented in the 85–175 km depth interval beneath the Kaapvaal Craton, in particular (Gibson, 2017). The highest shear-velocity anomalies are found at 100–200 km depths, varying with location, with maximum V_s values reaching 4.7–4.8 km/s, over 6% above the global average. The lithospheric thickness increases south to north, from $\sim$200 km beneath the central and southwestern Kaapvaal Craton to $\sim$300 km beneath the Limpopo Belt. The present lithospheric thickness in the west-central Kaapvaal is smaller than it was when sampled by Phanerozoic kimberlites ($\sim$260 km). This suggests that the lithosphere here has been thinned since the eruption of the kimberlites, possibly by the same hot mantle plume that gave rise to the numerous kimberlite eruptions. Topography in the Kaapvaal-Limpopo region varies in concert with the lithospheric thickness: higher elevations are where the lithosphere is thinner (central and southwestern Kaapvaal) and lower elevations are where the lithosphere is thicker (northern Kaapvaal and Limpopo). With the effect of the crustal structure on topography taken into account, the topography-lithospheric thickness relationship indicates that the deepest lithosphere beneath the Limpopo Belt (200–300 km depth range) is slightly to moderately depleted (Mg# 89.7–90.8).

Acknowledgments
The authors would like to thank an anonymous reviewer and the Editor, Ulrich Faul, for constructive, helpful suggestions. We also thank Balz Kamber, Emma Tomlinson, Saskia Goes, Nicolas Celli, Raffaele Bonadio, Pierre Arroucau and Mattia Guerri for insightful discussions and useful feedback. We are grateful to Celine Tirel who implemented Figure 11. This work was funded by the Dublin Institute for Advanced Studies and by Science Foundation Ireland (grant 13/CDA/2192). Acknowledgements go to the DJEI/DES/SFI/HEA Irish Centre for High-End-Computing (ICHEC) for the computational facilities and support. Figures 12 and 13 were prepared using the Generic Mapping Tool of Wessel and Smith (1998). The two station average dispersion measurements for the four regions of southern Africa can be obtained from https://homepages.dias.ie/~sergei/data/Ravenna_et_al_2018_data.txt.

References

Adam, J. M.-C. (2013). *Seismic structure and anisotropy in southern Africa's lithosphere: Constraints from broad-band surface-wave dispersion* (PhD thesis). Dublin, Ireland: Dublin Institute for Advanced Studies.

Adam, J. M.-C., & Lebedev, S. (2012). Azimuthal anisotropy beneath southern Africa from very broad-band surface-wave dispersion measurements. *Geophysical Journal International*, *191*, 155–174. https://doi.org/10.1111/j.1365-246X.2012.05583.x

Adams, A., & Nyblade, A. (2011). Shear wave velocity structure of the southern African upper mantle with implications for the uplift of southern Africa. *Geophysical Journal International*, *186*(2), 808–824. https://doi.org/10.1111/j.1365-246X.2011.05072.x

Afonso, J. C., Fernàndez, M., Ranalli, G., Griffin, W. L., & Connolly, J. A. D. (2008). Integrated geophysical-petrological modeling of the lithosphere and sublithospheric upper mantle: Methodology and applications. *Geochemistry, Geophysics, Geosystems*, *9*, Q05008. https://doi.org/10.1029/2007GC001834

Agius, M. R., & Lebedev, S. (2013). Tibetan and Indian lithospheres in the upper mantle beneath Tibet: Evidence from broadband surface-wave dispersion. *Geochemistry, Geophysics, Geosystems*, *14*, 4260–4281. https://doi.org/10.1002/ggge.20274

Agius, M. R., & Lebedev, S. (2014). Shear-velocity structure, radial anisotropy and dynamics of the Tibetan crust. *Geophysical Journal International*, *199*(3), 1395–1415. https://doi.org/10.1093/gji/ggu326

Argus, D. F., Gordon, R. G., & DeMets, C. (2011). Geologically current motion of 56 plates relative to the no-net-rotation reference frame. *Geochemistry, Geophysics, Geosystems*, *12*, Q11001. https://doi.org/10.1029/2011GC003751

Artemieva, I. M. (2009). The continental lithosphere: Reconciling thermal, seismic, and petrologic data. *Lithos*, *109*(1–2), 23–46. https://doi.org/10.1016/j.lithos.2008.09.015

Artemieva, I. M., & Vinnik, L. P. (2016). Density structure of the cratonic mantle in southern Africa: 1. Implications for dynamic topography. *Gondwana Research*, *39*, 204–216.

Bartzsch, S., Lebedev, S., & Meier, T. (2011). Resolving the lithosphere-asthenosphere boundary with seismic Rayleigh waves. *Geophysical Journal International*, *186*(3), 1152–1164. https://doi.org/10.1111/j.1365-246X.2011.05096.x

Bassin, C., Laske, G., & Masters, G. (2000). The current limits of resolution for surface wave tomography in North America. *Eos, Transactions American Geophysical Union*, *81*, F897.

Becker, T. W., Schaeffer, A. J., Lebedev, S., & Conrad, C. P. (2015). Toward a generalized plate motion reference frame. *Geophysical Research Letters*, *42*, 3188–3196. https://doi.org/10.1002/2015GL063695

Begg, G. C., Griffin, W. L., Natapov, L. M., O'Reilly, S. Y., Grand, S. P., O'Neill, C. J., et al. (2009). The lithospheric architecture of Africa: Seismic tomography, mantle petrology, and tectonic evolution. *Geosphere*, *5*(1), 23–50. https://doi.org/10.1130/GES00179.1

Beghein, C., & Trampert, J. (2004). Probability density functions for radial anisotropy: Implications for the upper 1200 km of the mantle. *Earth and Planetary Science Letters*, *217*(1–2), 151–162. https://doi.org/10.1016/S0012-821X(03)00575-2

Beghein, C., & Trampert, J. (2004). Probability density functions for radial anisotropy from fundamental mode surface wave data and the neighbourhood algorithm. *Geophysical Journal International*, *157*(3), 1163–1174. https://doi.org/10.1111/j.1365-246X.2004.02235.x

Bell, D. R., Grégoire, M., Grove, T. L., Chatterjee, N., Carlson, R. W., & Buseck, P. R. (2005). Silica and volatile-element metasomatism of Archean mantle: A xenolith-scale example from the Kaapvaal Craton. *Contributions to Mineralogy and Petrology*, *150*(3), 251–267. https://doi.org/10.1007/s00410-005-0673-8

Bloch, S., Hales, A., & Landisman, M. (1969). Velocities in the crust and upper mantle of southern Africa from multi-mode surface wave dispersion. *Bulletin of the Seismological Society of America*, *59*, 1599–1629.

Bonadio, R., Geissler, W., Lebedev, S., Fullea, J., Ravenna, M., Celli, N., et al. (2018). Hot upper mantle beneath the Tristan da Cunha Hotspot, from probabilistic Rayleigh-wave inversion and petrological modeling. *Geochemistry, Geophysics, Geosystems.* https://doi.org/10.1002/2017GC007347

Boyd, F. R., Gurney, J. J., & Richardson, S. H. (1985). Evidence for a 150–200-km thick Archaean lithosphere from diamond inclusion thermobarometry. *Nature*, *315*(6018), 387. http://doi.org/10.1038/315387a0

Boyd, F. R., & Mertzman, S. A. (1987). Composition of structure of the Kaapvaal lithosphere, southern Africa. *Magmatic Processes-Physiochemical Principles*, (I), 13–24.

Boyd, F. R., Pokhilenko, N. P., Pearson, D. G., Mertzman, S. A., Sobolev, N. V., & Finger, L. W. (1997). Composition of the Siberian cratonic mantle: Evidence from Udachnaya peridotite xenoliths. *Contributions to Mineralogy and Petrology*, *128*(2–3), 228–246. https://doi.org/10.1007/s004100050305

Bruneton, M., Pedersen, H. A., Vacher, P., Kukkonen, I. T., Arndt, N. T., Funke, S., et al. (2004). Layered lithospheric mantle in the central Baltic Shield from surface waves and xenolith analysis. *Earth and Planetary Science Letters*, *226*(1–2), 41–52. https://doi.org/10.1016/j.epsl.2004.07.034

Carlson, R. W., Boyd, F. R., Shirey, S. B., Janney, P. E., Grove, T. L., Bowring, S. A., et al. (2000). Continental growth, preservation, and modification in Southern Africa. *GSA Today*, *10*(2), 1–7.

Carlson, R. W., Grove, T. L., De Wit, M. J., & Gurney, J. J. (1996). Program to study crust and mantle of the Archean craton in southern Africa. *Eos, Transactions American Geophysical Union*, *77*(29), 273–277. https://doi.org/10.1029/96EO00194

Carlson, R. W., Pearson, D. G., Boyd, F. R., Shirey, S. B., Irvine, G., Menzies, A. H., et al. (1999). Re-Os systematics of Newlands peridotite xenoliths: Implications for diamond and lithosphere formation. In *Proceedings of the 7th International Kimberlite Conference* (pp. 99–108). Cape Town, South Africa.

Chang, S. J., Ferreira, A. M. G., Ritsema, J., Van Heijst, H. J., & Woodhouse, J. H. (2014). Global radially anisotropic mantle structure from multiple datasets: A review, current challenges, and outlook. *Tectonophysics*, *617*, 1. https://doi.org/10.1016/j.tecto.2014.01.033

Chang, S. J., Ferreira, A. M. G., Ritsema, J., van Heijst, H. J., & Woodhouse, J. H. (2015). Joint inversion for global isotropic and radially anisotropic mantle structure including crustal thickness perturbations. *Journal of Geophysical Research*, *120*, 4278–4300. https://doi.org/10.1002/2014JB011824

Chevrot, S., & Zhao, L. (2007). Multiscale finite-frequency Rayleigh wave tomography of the Kaapvaal Craton. *Geophysical Journal International*, *169*(1), 201–215. https://doi.org/10.1111/j.1365-246X.2006.03289.x

Christensen, N. I., & Mooney, W. D. (1995). Seismic velocity structure and composition of the continental crust: A global view. *Journal of Geophysical Research*, *100*(B6), 9761–9788. https://doi.org/10.1029/95JB00259

Cox, K. G. (1992). Karoo igneous activity, and the early stages of the break-up of Gondwanaland. *Geological Society Special Publications*, *68*(1), 137–148. https://doi.org/10.1144/GSL.SP.1992.068.01.09

Crampin, S. (1978). Seismic-wave propagation through a cracked solid: Polarization as a possible dilatancy diagnostic. *Geophysical Journal of the Royal Astronomical Society*, *53*(3), 467–496. https://doi.org/10.1111/j.1365-246X.1978.tb03754.x

Deen, T. J., Griffin, W. L., Begg, G., O'Reilly, S. Y., Natapov, L. M., & Hronsky, J. (2006). Thermal and compositional structure of the subcontinental lithospheric mantle: Derivation from shear wave seismic tomography. *Geochemistry, Geophysics, Geosystems*, *7*, Q07003. https://doi.org/10.1029/2005GC001120

De Wit, M. J. (1998). On Archean granites, greenstones, cratons and tectonics: Does the evidence demand a verdict? *Precambrian Research*, *91*(1–2), 181–226. https://doi.org/10.1016/S0301-9268(98)00043-6

Durrheim, R. J., & Mooney, W. D. (1991). Archaean and Proterozoic crustal evolution: Evidence from crustal seismology. *Geology*, *19*(6), 606–609.

Dziewonski, A. M., & Anderson, D. L. (1981). Preliminary reference Earth model. *Physics of the Earth and Planetary Interiors*, *25*(4), 297–356. https://doi.org/10.1016/0031-9201(81)90046-7

Eales, H. V., Marsh, J. S., & Cox, K. G. (1984). The Karoo igneous province: An introduction. *Special Publication of the Geological Society of South Africa*, *13*, 1–26.

Eaton, D. W., Darbyshire, F., Evans, R. L., Grütter, H., Jones, A. G., & Yuan, X. (2009). The elusive lithosphere-asthenosphere boundary (LAB) beneath cratons. *Lithos*, *109*(1–2), 1–22. https://doi.org/10.1016/j.lithos.2008.05.009

Endrun, B., Meier, T., Lebedev, S., Bohnhoff, M., Stavrakakis, G., & Harjes, H. P. (2008). S velocity structure and radial anisotropy in the Aegean region from surface wave dispersion. *Geophysical Journal International*, *174*(2), 593–616. https://doi.org/10.1111/j.1365-246X.2008.03802.x

Faul, U. H., & Jackson, I. (2005). The seismological signature of temperature and grain size variations in the upper mantle. *Earth and Planetary Science Letters*, *234*(1–2), 119–134. https://doi.org/10.1016/j.epsl.2005.02.008

Ferreira, A. M. G., Woodhouse, J. H., Visser, K., & Trampert, J. (2010). On the robustness of global radially anisotropic surface wave tomography. *Journal of Geophysical Research*, *115*, B04313. https://doi.org/10.1029/2009JB006716

Fishwick, S., & Reading, A. M. (2008). Anomalous lithosphere beneath the Proterozoic of western and central Australia: A record of continental collision and intraplate deformation? *Precambrian Research*, *166*(1–4), 111–121. https://doi.org/10.1016/j.precamres.2007.04.026

Flament, N., Gurnis, M., Williams, S., Seton, M., Skogseid, J., Heine, C., et al. (2014). Topographic asymmetry of the South Atlantic from global models of mantle flow and lithospheric stretching. *Earth and Planetary Science Letters*, *387*, 107–119. https://doi.org/10.1016/j.epsl.2013.11.017

Fouch, M. J., James, D. E., Vandecar, J. C., & van der Lee, S. (2004). Mantle seismic structure beneath the Kaapvaal and Zimbabwe Cratons. *South African Journal of Geology*, *107*(1–2), 33–44.

French, S. W., & Romanowicz, B. (2015). Broad plumes rooted at the base of the Earth's mantle beneath major hotspots. *Nature*, *525*(7567), 95. http://doi.org/10.1038/nature14876

Freybourger, M., Gaherty, J. B., & Jordan, T. H. (2001). Structure of the Kaapvaal Craton from surface waves. *Geophysical Research Letters*, *28*(13), 2489–2492. https://doi.org/10.1029/2000GL012436

Fullea, J., Afonso, J. C., Connolly, J. A. D., Fernàndez, M., García-Castellanos, D., & Zeyen, H. (2009). LitMod3D: An interactive 3-D software to model the thermal, compositional, density, seismological, and rheological structure of the lithosphere and sublithospheric upper mantle. *Geochemistry, Geophysics, Geosystems*, *10*, Q08019. https://doi.org/10.1029/2009GC002391

Fullea, J., Lebedev, S., Agius, M. R., Jones, A. G., & Afonso, J. C. (2012). Lithospheric structure in the Baikal-central Mongolia region from integrated geophysical-petrological inversion of surface-wave data and topographic elevation. *Geochemistry, Geophysics, Geosystems*, *13*, Q0AK09. https://doi.org/10.1029/2012GC004138

Fullea, J., Muller, M. R., & Jones, A. G. (2011). Electrical conductivity of continental lithospheric mantle from integrated geophysical and petrological modeling: Application to the Kaapvaal Craton and Rehoboth Terrane, southern Africa. *Journal of Geophysical Research*, *116*, B10202. https://doi.org/10.1029/2011JB008544

Gaherty, J. B., & Jordan, T. H. (1995). Lehmann discontinuity as the base of an anisotropic layer beneath continents. *Science*, *268*(5216), 1468–1471. https://doi.org/10.1126/science.268.5216.1468

Gibson, S. (2017). On the nature and origin of garnet in highly-refractory Archean lithospheric mantle: Constraints from garnet exsolved in Kaapvaal Craton orthopyroxenes. *Mineralogical Magazine*, *81*(4), 781–809. https://doi.org/10.1180/minmag.2016.080.158

Gore, J., James, D. E., Zengeni, T. G., & Gwavava, O. (2009). Crustal structure of the Zimbabwe Craton and the Limpopo Belt of Southern Africa: New constraints from seismic data and implications for its evolution. *South African Journal of Geology*, *112*(3–4), 213–228.

Grand, S. P., & Helmberger, D. V. (1984). Upper mantle shear structure of North America. *Geophysical Journal International*, *76*(2), 399–438. https://doi.org/10.1111/j.1365-246X.1984.tb05053.x

Green, R. W. E., & Hales, A. L. (1968). The travel times of P waves to 30° in the central United States and upper mantle structure. *Bulletin of the Seismological Society of America*, *58*(1), 267–289.

Griffin, W. L., Graham, S., O'Reilly, S. Y., & Pearson, N. J. (2004). Lithosphere evolution beneath the Kaapvaal Craton: Re-Os systematics of sulfides in mantle-derived peridotites. *Chemical Geology*, *208*(1–4), 89–118. https://doi.org/10.1016/j.chemgeo.2004.04.007

Griffin, W. L., O'Reilly, S. Y., & Ryan, C. G. (1999). The composition and origin of subcontinental lithospheric mantle. In Fei, Y., Bertka, C. M., & Mysen, B. O. (Eds.), *Mantle petrology: Field observations and high-pressure experimentation: A tribute to Francis R. (Joe) Boyd*. *Geochemical Society Special Publication*, 6, 13–45.

Griffin, W. L., O'Reilly, S. Y., Natapov, L. M., & Ryan, C. G. (2003). The evolution of lithospheric mantle beneath the Kalahari Craton and its margins. *Lithos*, *71*(2–4), 215–241. https://doi.org/10.1016/j.lithos.2003.07.006

Gripp, A. E., & Gordon, R. G. (1990). Current plate velocities relative to the hotspots incorporating the NUVEL-1 global plate motion model. *Geophysical Research Letters*, *17*(8), 1109–1112. https://doi.org/10.1029/GL017i008p01109

Grütter, H., Latti, D., & Menzies, A. (2006). Cr-saturation arrays in concentrate garnet compositions from kimberlite and their use in mantle barometry. *Journal of Petrology*, *47*(4), 801–820. https://doi.org/10.1093/petrology/egi096

Gung, Y., Panning, M., & Romanowicz, B. (2003). Global anisotropy and the thickness of continents. *Nature*, *422*(6933), 707–711. https://doi.org/10.1038/nature01559

Gurnis, M., Mitrovica, J. X., Ritsema, J., & Van Heijst, H. J. (2000). Constraining mantle density structure using geological evidence of surface uplift rates: The case of the African Superplume. *Geochemistry, Geophysics, Geosystems*, *1*(7), 1020. https://doi.org/10.1029/1999GC000035

Gwavava, O., Swain, C. J., Podmore, F., & Fairhead, J. D. (1992). Evidence of crustal thinning beneath the Limpopo Belt and Lebombo monocline of southern Africa based on regional gravity studies and implications for the reconstruction of Gondwana. *Tectonophysics*, *212*(1–2), 1–20.

Hacker, B. R., Kelemen, P. B., & Behn, M. D. (2015). Continental lower crust. *Annual Review of Earth and Planetary Sciences*, *43*(1), 167–205. https://doi.org/10.1146/annurev-earth-050212-124117

Hager, B. H., Clayton, R. W., Richards, M. A., Comer, R. P., & Dziewonski, A. M. (1985). Lower mantle heterogeneity, dynamic topography and the geoid. *Nature*, *313*(6003), 541–545. https://doi.org/10.1038/313541a0

Hales, A. L. (1969). A seismic discontinuity in the lithosphere. *Earth and Planetary Science Letters*, *7*(1), 44–46. https://doi.org/10.1016/0012-821X(69)90009-0

Hansen, S. E., Nyblade, A. A., Julià, J., Dirks, P. H. G. M., & Durrheim, R. J. (2009). Upper-mantle low-velocity zone structure beneath the Kaapvaal Craton from S-wave receiver functions. *Geophysical Journal International*, *178*(2), 1021–1027. https://doi.org/10.1111/j.1365-246X.2009.04178.x

Hieronymus, C. F., & Goes, S. (2010). Complex cratonic seismic structure from thermal models of the lithosphere: Effects of variations in deep radiogenic heating. *Geophysical Journal International*, *180*(3), 999–1012. https://doi.org/10.1111/j.1365-246X.2009.04478.x

Hirsch, A. C., Dalton, C. A., & Ritsema, J. (2015). Constraints on shear velocity in the cratonic upper mantle from Rayleigh wave phase velocity. *Geochemistry, Geophysics, Geosystems*, *16*, 3982–4005. https://doi.org/10.1002/2015GC006066

Hofmann, A., Kröner, A., & Brandl, G. (1998). Field relationships of mid- to late Archaean high-grade gneisses of igneous and sedimentary parentage in the Sand River, Central Zone of the Limpopo Belt, South Africa. *South African Journal of Geology*, *101*(3), 185–200.

Holzer, L., Frei, R., Barton, J. M., & Kramers, J. D. (1998). Unraveling the record of successive high grade events in the Central Zone of the Limpopo Belt using Pb single phase dating of metamorphic minerals. *Precambrian Research*, *87*(1–2), 87–115. https://doi.org/10.1016/S0301-9268(97)00058-2

James, D. E., Boyd, F. R., Schutt, D., Bell, D. R., & Carlson, R. W. (2004). Xenolith constraints on seismic velocities in the upper mantle beneath southern Africa. *Geochemistry, Geophysics, Geosystems*, *5*, Q01002. https://doi.org/10.1029/2003GC000551

James, D. E., Fouch, M. J., VanDecar, J. C., & van der Lee, S. (2001). Tectospheric structure beneath southern Africa. *Geophysical Research Letters*, *28*(13), 2485–2488. https://doi.org/10.1029/2000GL012578

Jones, A. G., Afonso, J. C., & Fullea, J. (2017). Geochemical and geophysical constrains on the dynamic topography of the Southern African Plateau. *Geochemistry, Geophysics, Geosystems*, *18*, 3556–3575. https://doi.org/10.1002/2017GC006908

Jordan, T. H. (1975). The continental tectosphere. *Reviews of Geophysics*, *13*(3), 1–12. https://doi.org/10.1029/RG013i003p00001

Jordan, T. H. (1988). Structure and formation of the continental tectosphere. *Journal of Petrology*, *Special_Volume*(1), 11–37.

Kamber, B. S. (2015). The evolving nature of terrestrial crust from the Hadean, through the Archaean, into the Proterozoic. *Precambrian Research*, *258*, 48–82. https://doi.org/10.1016/j.precamres.2014.12.007

Kamber, B. S., Kramers, J. D., Napier, R., Cliff, R. A., & Rollinson, H. R. (1995). The Triangle Shearzone, Zimbabwe, revisited: New data document an important event at 2.0 Ga in the Limpopo Belt. *Precambrian Research*, *70*(3–4), 191–213. https://doi.org/10.1016/0301-9268(94)00039-T

Kennett, B. L. N., Engdahl, E. R., & Buland, R. (1995). Constraints on seismic velocities in the Earth from traveltimes. *Geophysical Journal International*, *122*(1), 108–124. https://doi.org/10.1111/j.1365-246X.1995.tb03540.x

Khan, A., Zunino, A., & Deschamps, F. (2013). Upper mantle compositional variations and discontinuity topography imaged beneath Australia from Bayesian inversion of surface-wave phase velocities and thermochemical modeling. *Journal of Geophysical Research: Solid Earth*, *118*, 5285–5306. https://doi.org/10.1002/jgrb.50304

Klemme, S. (2004). The influence of Cr on the garnet-spinel transition in the Earth's mantle: Experiments in the system MgO-Cr_2O_3-SiO_2 and thermodynamic modelling. *Lithos*, *77*(1–4), 639–646. https://doi.org/10.1016/j.lithos.2004.03.017

Klemme, S., Ivanic, T. J., Connolly, J. A. D., & Harte, B. (2009). Thermodynamic modelling of Cr-bearing garnets with implications for diamond inclusions and peridotite xenoliths. *Lithos*, *112*, 986–991. https://doi.org/10.1016/j.lithos.2009.05.007

Kopylova, M. G., & Caro, G. (2004). Mantle xenoliths from the Southeastern Slave Craton: Evidence for chemical zonation in a thick, cold lithosphere. *Journal of Petrology*, *45*(5), 1045–1067. https://doi.org/10.1093/petrology/egh003

Larson, A. M., Snoke, J. A., & James, D. E. (2006). S-wave velocity structure, mantle xenoliths and the upper mantle beneath the Kaapvaal Craton. *Geophysical Journal International*, *167*(1), 171–186. http://doi.org/10.1111/j.1365-246X.2006.03005.x

Lebedev, S., Adam, J. M.-C., & Meier, T. (2013). Mapping the Moho with seismic surface waves: A review, resolution analysis, and recommended inversion strategies. *Tectonophysics*, *609*, 377–394. https://doi.org/10.1016/j.tecto.2012.12.030

Lebedev, S., Boonen, J., & Trampert, J. (2009). Seismic structure of Precambrian lithosphere: New constraints from broad-band surface-wave dispersion. *Lithos*, *109*(1–2), 96–111. https://doi.org/10.1016/j.lithos.2008.06.010

Lebedev, S., Meier, T., & van der Hilst, R. D. (2006). Asthenospheric flow and origin of volcanism in the Baikal Rift area. *Earth and Planetary Science Letters*, *249*(3–4), 415–424. https://doi.org/10.1016/j.epsl.2006.07.007

Lebedev, S., Nolet, G., Meier, T., & van der Hilst, R. D. (2005). Automated multimode inversion of surface and S waveforms. *Geophysical Journal International*, *162*(3), 951–964. https://doi.org/10.1111/j.1365-246X.2005.02708.x

Lebedev, S., Schaeffer, A. J., Fullea, J., & Pease, V. (2018). Seismic tomography of the Arctic region: Inferences for the thermal structure and evolution of the lithosphere. In Pease, V. & Coakley, B. (Eds.), *Circum-Arctic lithosphere evolution*. *Geological Society Special Publications*, 419–440. https://doi.org/10.1144/SP460.10

Lebedev, S., & van der Hilst, R. D. (2008). Global upper mantle tomography with the automated multimode inversion of surface and S wave forms. *Geophysical Journal International*, *173*(2), 505–518. http://doi.org/10.1111/j.1365-246X.2008.03721.x

Lee, C.-T. A. (2003). Compositional variation of density and seismic velocities in natural peridotites at STP conditions: Implications for seismic imaging of compositional heterogeneities in the upper mantle. *Journal of Geophysical Research*, *108*(B9), 2441. https://doi.org/10.1029/2003JB002413

Legendre, C. P., Meier, T., Lebedev, S., Friederich, W., & Viereck-Götte, L. (2012). A shear wave velocity model of the European upper mantle from automated inversion of seismic shear and surface waveforms. *Geophysical Journal International*, *191*(1), 282–304. https://doi.org/10.1111/j.1365-246X.2012.05613.x

Li, A., & Burke, K. (2006). Upper mantle structure of southern Africa from Rayleigh wave tomography. *Journal of Geophysical Research*, *111*, B10303. https://doi.org/10.1029/2006JB004321

Lithgow-Bertelloni, C., & Silver, P. (1998). Dynamic topography, plate driving forces and the African superswell. *Nature*, *395*(6699), 269–348.https://doi.org/10.1038/26212

Meier, T., Dietrich, K., Stöckhert, B., & Harjes, H. P. (2004). One-dimensional models of shear wave velocity for the eastern Mediterranean obtained from the inversion of Rayleigh wave phase velocities and tectonic implications. *Geophysical Journal International*, *156*(1), 45–58. https://doi.org/10.1111/j.1365-246X.2004.02121.x

Meier, T., Soomro, R. A., Viereck, L., Lebedev, S., Behrmann, J. H., Weidle, C., et al. (2016). Mesozoic and Cenozoic evolution of the Central European lithosphere. *Tectonophysics*, *692*, 58–73. https://doi.org/10.1016/j.tecto.2016.09.016

Moschetti, M. P., Ritzwoller, M. H., Lin, F., & Yang, Y. (2010). Seismic evidence for widespread western-US deep-crustal deformation caused by extension. *Nature*, *464*(7290), 885. http://doi.org/10.1038/nature08951

Muller, M., Fullea, J., Jones, A., Adam, J. M.-C., Lebedev, S., & Agostinetti, N. (2013). Lithospheric-Mantle structure of the Kaapvaal Craton, South Africa, derived from thermodynamically self-consistent modelling of magnetotelluric, surface-wave dispersion, S-wave receiver function, heat-flow, elevation and xenolith observations. *In Geophys. Res. Abst*, *15*, (Vol.). EGU2013–12903, EGU General Assembly 2013.

Müller, R. D., Sdrolias, M., Gaina, C., & Roest, W. R. (2008). Age, spreading rates, and spreading asymmetry of the world's ocean crust. *Geochemistry, Geophysics, Geosystems*, *9*, Q04006. https://doi.org/10.1029/2007GC001743

Nair, S. K., Gao, S. S., Liu, K. H., & Silver, P. G. (2006). Southern African crustal evolution and composition: Constraints from receiver function studies. *Journal of Geophysical Research*, *111*, B02304. https://doi.org/10.1029/2005JB003802

Nettles, M., & Dziewoński, A. M. (2008). Radially anisotropic shear velocity structure of the upper mantle globally and beneath North America. *Journal of Geophysical Research*, *113*, B02303. https://doi.org/10.1029/2006JB004819

Nguuri, T. K., Gore, J., James, D. E., Webb, S. J., Wright, C., Zengeni, T. G., et al. (2001). Crustal structure beneath southern Africa and its implications for the formation and evolution of the Kaapvaal and Zimbabwe cratons. *Geophysical Research Letters*, *28*(13), 2501–2504. https://doi.org/10.1029/2000GL012587

Nur, A. (1971). Effects of stress on velocity anisotropy in rocks with cracks. *Journal of Geophysical Research*, *76*(8), 2022–2034. https://doi.org/10.1029/JB076i008p02022

Nyblade, A. A., & Robinson, S. W. (1994). The African Superswell. *Geophysical Research Letters*, *21*(9), 765–768. https://doi.org/10.1029/94GL00631

O'Reilly, S. Y., & Griffin, W. L. (2006). Imaging global chemical and thermal heterogeneity in the subcontinental lithospheric mantle with garnets and xenoliths: Geophysical implications. *Tectonophysics*, *416*(1–4), 289–309. https://doi.org/10.1016/j.tecto.2005.11.014

Pearson, D. G., Carlson, R. W., Shirey, S. B., Boyd, F. R., & Nixon, P. H. (1995). Stabilisation of Archaean lithospheric mantle: A ReOs isotope study of peridotite xenoliths from the Kaapvaal Craton. *Earth and Planetary Science Letters*, *134*(3–4), 341–357. https://doi.org/10.1016/0012-821X(95)00125-V

Pedersen, H. A., Fishwick, S., & Snyder, D. B. (2009). A comparison of cratonic roots through consistent analysis of seismic surface waves. *Lithos*, *109*(1–2), 81–95. https://doi.org/10.1016/j.lithos.2008.09.016

Priestley, K. (1999). Velocity structure of the continental upper mantle: Evidence from southern Africa. *Lithos*, *48*(1–4), 45–56. https://doi.org/10.1016/S0024-4937(99)00021-3

Priestley, K., McKenzie, D., & Debayle, E. (2006). The state of the upper mantle beneath southern Africa. *Tectonophysics*, *416*(1–4), 101–112. https://doi.org/10.1016/j.tecto.2005.11.024

Priestley, K., & Tilmann, F. (2009). Relationship between the upper mantle high velocity seismic lid and the continental lithosphere. *Lithos*, *109*(1–2), 112–124. https://doi.org/10.1016/j.lithos.2008.10.021

Qiu, X., Priestley, K., & McKenzie, D. (1996). Average lithospheric structure of southern Africa. *Geophysical Journal International*, *127*(3), 563–587. https://doi.org/10.1111/j.1365-246X.1996.tb04038.x

Ravenna, M., & Lebedev, S. (2018). Bayesian inversion of surface-wave data for radial and azimuthal shear-wave anisotropy, with applications to central Mongolia and west-central Italy. *Geophysical Journal International*, *213*(1), 278–300. https://doi.org/10.1093/gji/ggx497

Ravenna, M., Lebedev, S., & Adam, J. M.-C. (2017). Shear-velocity structure and azimuthal and radial anisotropy beneath the Kaapvaal Craton from Bayesian inversion of surface-wave data: Inferences for the architecture and early evolution of cratons. In *AGU conference abstract*. Washington, DC: American Geophysical Union.

Revenaugh, J., & Jordan, T. H. (1991). Mantle layering from ScS reverberations: 3. The upper mantle. *Journal of Geophysical Research*, *96*(B12), 19781–19810. https://doi.org/10.1029/91JB01487

Ritsema, J., van Heijst, H. J., & Woodhouse, J. H. (1999). Complex shear wave velocity structure imaged beneath Africa and Iceland. *Science*, *286*(5446), 1925–1928. https://doi.org/10.1126/science.286.5446.1925

Romanowicz, B., & Gung, Y. (2002). Superplumes from the core-mantle boundary to the lithosphere: Implications for heat flux. *Science*, *296*(5567), 513–516. https://doi.org/10.1126/science.1069404

Saltzer, R. L. (2002). Upper mantle structure of the Kaapvaal Craton from surface wave analysis—A second look. *Geophysical Research Letters*, *29*(6). https://doi.org/10.1029/2001GL013702

Saltzer, R. L., Chatterjee, N., & Grove, T. L. (2001). The spatial distribution of garnets and pyroxenes in mantle peridotites: Pressure-temperature history of peridotites from the Kaapvaal Craton. *Journal of Petrology*, *42*(12), 2215–2229. https://doi.org/10.1093/petrology/42.12.2215

Schaeffer, A. J., & Lebedev, S. (2015). Global heterogeneity of the lithosphere and underlying mantle: A seismological appraisal based on multimode surface-wave dispersion analysis, shear-velocity tomography, and tectonic regionalization. In Khan, A., & Deschamps, F. (Eds.), *The Earth's heterogeneous mantle. Springer Geophysics*. Cham: Springer.

Schutt, D. L., & Lesher, C. E. (2006). Effects of melt depletion on the density and seismic velocity of garnet and spinel lherzolite. *Journal of Geophysical Research*, *111*, B05401. https://doi.org/10.1029/2003JB002950

Schutt, D. L., & Lesher, C. E. (2010). Compositional trends among Kaapvaal Craton garnet peridotite xenoliths and their effects on seismic velocity and density. *Earth and Planetary Science Letters*, *300*(3–4), 367–373. https://doi.org/10.1016/j.epsl.2010.10.018

Shapiro, N. M., & Ritzwoller, M. H. (2002). Monte-Carlo inversion for a global shear velocity model of the crust and upper mantle. *Geophysical Journal International*, *151*(1), 88–105. https://doi.org/10.1046/j.1365-246X.2002.01742.x

Shapiro, N. M., & Ritzwoller, M. H. (2004). Thermodynamic constraints on seismic inversions. *Geophysical Journal International*, *157*(3), 1175–1188. https://doi.org/10.1111/j.1365-246X.2004.02254.x

Shapiro, N. M., Ritzwoller, M. H., Mareschal, J. C., & Jaupart, C. (2004). Lithospheric structure of the Canadian Shield inferred from inversion of surface-wave dispersion with thermodynamic a priori constraints. *Geological Society Special Publications*, *239*(1), 175–194. https://doi.org/10.1144/GSL.SP.2004.239.01.12

Simon, N. S. C., Irvine, G. J., Davies, G. R., Pearson, D. G., & Carlson, R. W. (2003). The origin of garnet and clinopyroxene in "depleted" Kaapvaal peridotites. *Lithos*, *71*(2–4), 289–322. https://doi.org/10.1016/S0024-4937(03)00118-X

Sobolev, S. V., Sobolev, A. V., Kuzmin, D. V., Krivolutskaya, N. A., Petrunin, A. G., Arndt, N. T., et al. (2011). Linking mantle plumes, large igneous provinces and environmental catastrophes. *Nature*, *477*(7364), 312–316. https://doi.org/10.1038/nature10385

Sodoudi, F., Yuan, X., Kind, R., Lebedev, S., Adam, J. M.-C., Kästle, E., et al. (2013). Seismic evidence for stratification in composition and anisotropic fabric within the thick lithosphere of Kalahari Craton. *Geochemistry, Geophysics, Geosystems*, *14*, 5393–5412. https://doi.org/10.1002/2013GC004955

Soomro, R. A., Weidle, C., Cristiano, L., Lebedev, S., & Meier, T., & PASSEQ working group (2016). Phase velocities of Rayleigh and Love waves in central and northern Europe from automated, broad-band, interstation measurements. *Geophysical Journal International*, *204*(1), 517–534. https://doi.org/10.1093/gji/ggv462

Stein, C. A., & Stein, S. (1992). A model for the global variation in oceanic depth and heat flow with lithospheric age. *Nature*, *359*(6391), 123. http://doi.org/10.1038/359123a0

Stixrude, L., & Lithgow-Bertelloni, C. (2005). Mineralogy and elasticity of the oceanic upper mantle: Origin of the low-velocity zone. *Journal of Geophysical Research*, *110*, B03204. https://doi.org/10.1029/2004JB002965

Tomlinson, E. L., Kamber, B. S., Hoare, B. C., Stead, C. V., & Ildefonse, B. (2017). An exsolution origin for Archean mantle garnet. *Geology*, *46*(2), 123–126. https://doi.org/10.1130/G39680.1

van der Hilst, R. D., Widiyantoro, S., & Engdahl, E. R. (1997). Evidence for deep mantle circulation from global tomography. *Nature*, *386*(6625), 578. http://doi.org/10.1038/386578a0

Visser, K., Trampert, J., Lebedev, S., & Kennett, B. L. N. (2008). Probability of radial anisotropy in the deep mantle. *Earth and Planetary Science Letters*, *270*(3–4), 241–250. https://doi.org/10.1016/j.epsl.2008.03.041

Vozar, J., Jones, A. G., Fullea, J., Agius, M. R., Lebedev, S., Pape, F., et al. (2014). Integrated geophysical-petrological modeling of lithosphere-asthenosphere boundary in central Tibet using electromagnetic and seismic data. *Geochemistry, Geophysics, Geosystems*, *15*, 3965–3988. https://doi.org/10.1002/2014GC005365

Walter, M. J. (1998). Melting of garnet peridotite and the origin of komatiite and depleted lithosphere. *Journal of Petrology*, *39*(1), 29–60. https://doi.org/10.1093/petrology/39.1.29

Wessel, P., & Smith, W. H. F. (1998). New, improved version of generic mapping tools released. *Eos, Transactions American Geophysical Union*, *79*(47), 579. https://doi.org/10.1029/98EO00426

Wittlinger, G., & Farra, V. (2007). Converted waves reveal a thick and layered tectosphere beneath the Kalahari super-craton. *Earth and Planetary Science Letters*, *254*(3–4), 404–415. https://doi.org/10.1016/j.epsl.2006.11.048

Yang, Y., Li, A., & Ritzwoller, M. H. (2008). Crustal and uppermost mantle structure in southern Africa revealed from ambient noise and teleseismic tomography. *Geophysical Journal International*, *174*(1), 235–248. https://doi.org/10.1111/j.1365-246X.2008.03779.x

Youssof, M., Thybo, H., Artemieva, I. M., & Levander, A. (2013). Moho depth and crustal composition in Southern Africa. *Tectonophysics*, *609*(Suppl. C), 267–287. https://doi.org/10.1016/j.tecto.2013.09.001

Zhao, M., Langston, C. A., Nyblade, A. A., & Owens, T. J. (1999). Upper mantle velocity structure beneath southern Africa from modeling regional seismic data. *Journal of Geophysical Research*, *104*(B3), 4783–4794. https://doi.org/10.1029/1998JB900058

Ziberna, L., Klemme, S., & Nimis, P. (2013). Garnet and spinel in fertile and depleted mantle: Insights from thermodynamic modelling. *Contributions to Mineralogy and Petrology*, *166*(2), 411–421. https://doi.org/10.1007/s00410-013-0882-5